EVALUATING THE SINTERING OF GLASS FRITS USING
HOT STAGE MICROSCOPY

BY

MACKENZIE N. STEVENS

A THESIS

SUBMITTED TO THE FACULTY OF

ALFRED UNIVERSITY

IN PARTIAL FULFILLMENT OF THE REQUIREMENTS

FOR THE DEGREE OF

MASTER OF SCIENCE

IN

CERAMIC ENGINEERING

ALFRED, NEW YORK

SEPTEMBER 2021

EVALUATING THE SINTERING OF GLASS FRIT USING HOT
STAGE MICROSCOPY

BY

MACKENZIE N. STEVENS

B.S. UNIVERSITY OF PITTSBURGH (2017)

SIGNATURE OF AUTHOR _____

APPROVED BY_____
      WILLIAM M. CARTY, ADVISOR

_____
WILLIAM LACOURSE, ADVISORY COMMITTEE

_____
YIQUAN WU, ADVISORY COMMITTEE

_____
WILLIAM CARLSON, CHAIR, ORAL THESIS DEFENSE

ACCEPTED BY _____
     GABRIELLE G. GAUSTAAD, DEAN
KAZUO INAMORI SCHOOL OF ENGINEERING

ACKNOWLEDGMENTS

TABLE OF CONTENTS

LIST OF TABLES

LIST OF FIGURES

ABSTRACT

This study uses the direct observation of the heating of cylindrical powder compacts via hot-stage microscope (HSM), with heating rates from 1.0 to 60 K/min, to establish sintering ranges and activation energies of three glasses. The HSM allows the quick and simple thermo-analytical examination of macroscopic sintering behavior, using small samples (approximately 12.8 mm^3) to minimize heat transfer problems. The use of mechanically pressed compacts with similar initial densities allows for the comparison of densification behavior of samples subjected to different heating rates. The sintering of glass powders, recognized to occur through the bulk transport mechanism of viscous flow, subsumes several caveats when comparing theory to experimental observation. The densification of powder particles as they coalesce into a monolith will occur over a temperature range >100 K during non-isothermal heat treatments. The densification temperature, defined as the peak in the shrinkage curve, increased with increasing heating rates. Heat work, defined as the accumulation of thermal energy with time (K·s), is proposed to have a dependence on the logarithm of time when calculated from the glass transition temperature to the sintering temperature. Heat work is constant for two of the glasses, but decreases with increasing heating rate for the investigated borosilicate glass. Activation energies were calculated and are similar to published values.

INTRODUCTION

Glass parts are normally formed from casting, drawing or working/blowing molten glass. These methods require low glass viscosities and are limited in shape; complexity for cast and drawn parts, reproducibility for blown parts. Additionally contact between the glass and the cast surfaces or tooling, e.g., rollers and pliers, introduce surface flaws that may require grinding and polishing, which can be difficult and expensive.[1] High temperatures are required to reduce the viscosity of glass to where glass forming liquids may be useful in industry for pouring or gathering and working.[2] Lower viscosities allow for more reasonable timescales for batch reactions and fining of glass (chemical homogenization and the removal of bubbles and seeds). After melts are homogenized, glass-forming liquids are formed to the desired shape and quickly cooled. Subsequent annealing is required to relieve internal residual stress that arises from fast cooling. Glass frit sintering allows the opportunity for complex shape production. For example, glass parts used in hermetic sealing applications can, as of today, only be produced via sintering glass frit powder compacts. Lower processing temperatures, as those used in sintering, avoid low viscosity glass flow, thus retaining the net shape of the initial form. Sintering allows for novel processing techniques, such as 3D printing, to manufacture intricate geometries, without the need for machining.

Glass is known to sinter via viscous flow, a bulk transport phenomenon first described by Frenkel as an energy balance between the reduction in surface energy and the driving force for sintering.[3] Frenkel's energy balance concept is the foundation of viscous flow and glass sintering models. Mackenzie and Shuttleworth proposed a theory to describe the final stages of sintering based on the surface tension of closed pores.[4] These classical sintering theories assume spherical, monosized particles (and pores), and are applicable under isothermal sintering conditions, i.e., heat treatments that occur at a fixed temperature.[3-6] While these assumptions simplify calculations, they may not accurately reflect the behavior of irregularly shaped particles obtained by the comminution of glass frits. More importantly, glass sintering is usually not conducted under isothermal conditions. Since sintering occurs over a wide range of temperatures, the kinetics of viscous flow may be influenced by heating rate.[7] Slower heating rates will allow for viscous flow

1

to take place over a longer period of time such that maximum density may be reached at lower temperatures. Faster heating rates require more time for thermal equilibrium within the sample, and thus, may not reach its maximum sintered density until higher temperatures.

One of the considerations in this investigation was the potential effect of radiation absorption, based on the color differences of the frits, on sintering behavior. However, Figure 1 illustrates similar absorption behavior in the infrared region of the white and blue glasses examined in this study. Therefore, the observed sintering temperatures suggest approximately equal dependence on heating rate of the system. The absorption spectrum is similar and therefore radiation is not expected to contribute to the sintering behavior of the glasses.
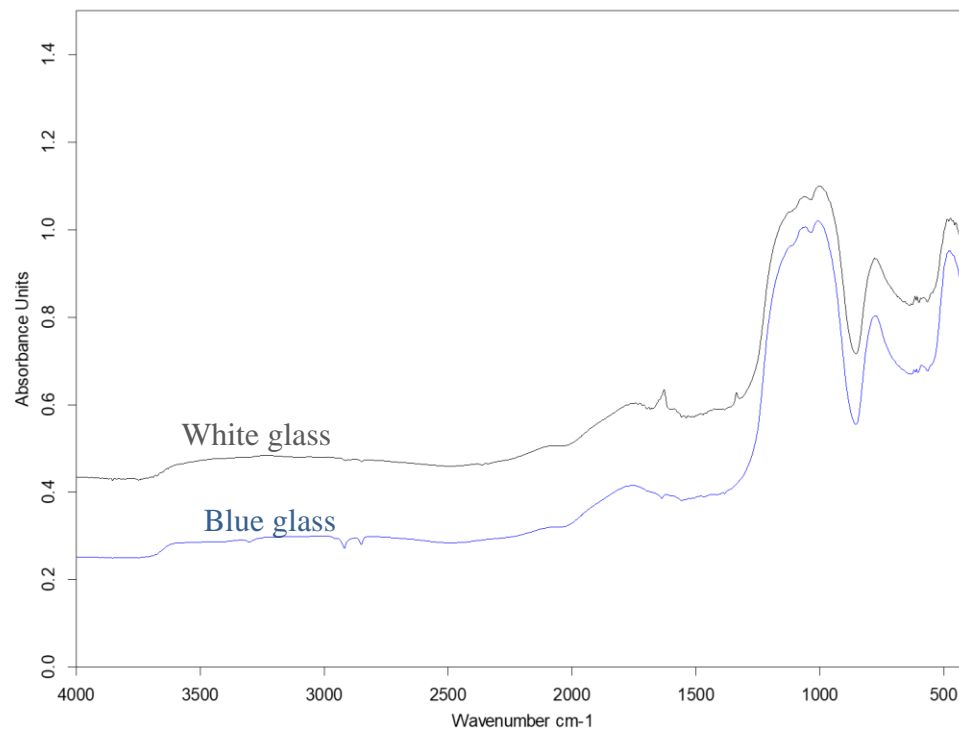
Figure 1. FTIR analysis of white and blue glass measured in absorption.

Borosilicate glasses are expected to exhibit different sintering behavior compared to silicate glasses based on their viscosity-temperature relations. Sintering has been proposed to occur at a specific viscosity.[8-9] Viscosity of a typical soda-lime silicate container glass (SLS) decreases more rapidly with increasing temperature than a typical borosilicate glass, as demonstrated in Figure 2.[10] Therefore, a borosilicate glass may sinter

at higher temperatures (in relation to the glass transition temperature) than SLS, if sintering viscosity occurs below 10^{11} Pa.s, which has been confirmed.[8, 11-13] Therefore, it is of interest to compare the sintering behavior of borosilicate and silicate glasses.
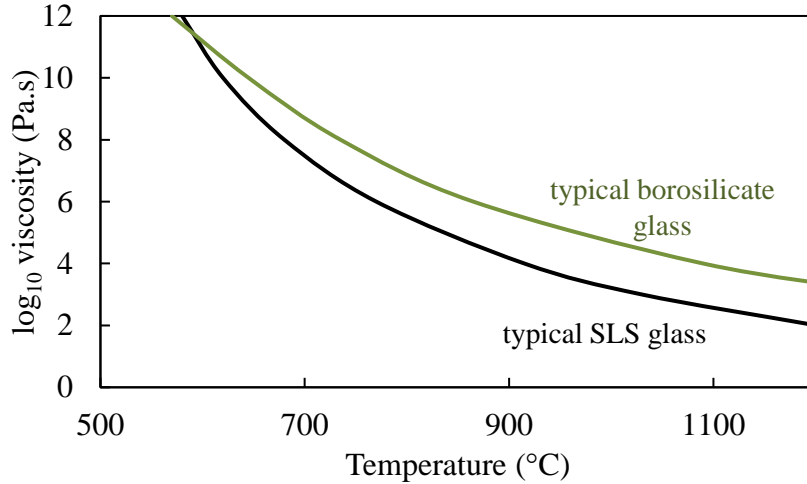
Figure 2. Viscosity-temperature curves for typical soda-lime-silicate glass and a low-expansion borosilicate glass, replotted from Fluegel.[10, 14]

Introduction to Hot-stage Microscopy

According to Mackenzie and Shuttleworth,[4] viscous flow happens on a macroscopic scale, allowing the examination of volumetric shrinkage and shape deformation. Therefore, a simple experiment using a heating microscope may appropriately describe viscous flow, the mechanism responsible for the sintering of glass. The hot-stage microscope (HSM) is an effective technique for observing the sintering and melting behavior of glasses.[8, 11, 15-17] Measuring the shrinkage, or the densification, of a powder compact is an efficient and repeatable method for studying sintering. The HSM accurately measures dimensional changes *in-situ*, illuminating the sintering process while evaluating the effects of process variables, such as heating rate and pressed density. Sample dimensions are automatically quantified at allocated temperature or time increments to collect data that otherwise must be manually and painstakingly measured. The HSM is capable of a broad range of heating rates, from 1 to 80 K/min. Faster heating rates, such as 80 K/min, may reasonably represent the condition when a sample is placed directly into a hot furnace.[17]

The HSM captures the silhouette of the sample such that a three-dimensional cylindrical sample can be simplified and analyzed as a two-dimensional rectangle. The

3

number of pixels within the silhouette are quantified to determine changes in area with time or temperature, reported as 'area variance.' An example of the differing shape morphologies captured by HSM with respect to temperature and subjected to various heating rates is displayed in Figure 3. Experimenting with various heating rates can determine if sintering occurs at a specific temperature or once the system overcomes a thermal energy barrier based on time at temperature; a concept known as heat work.
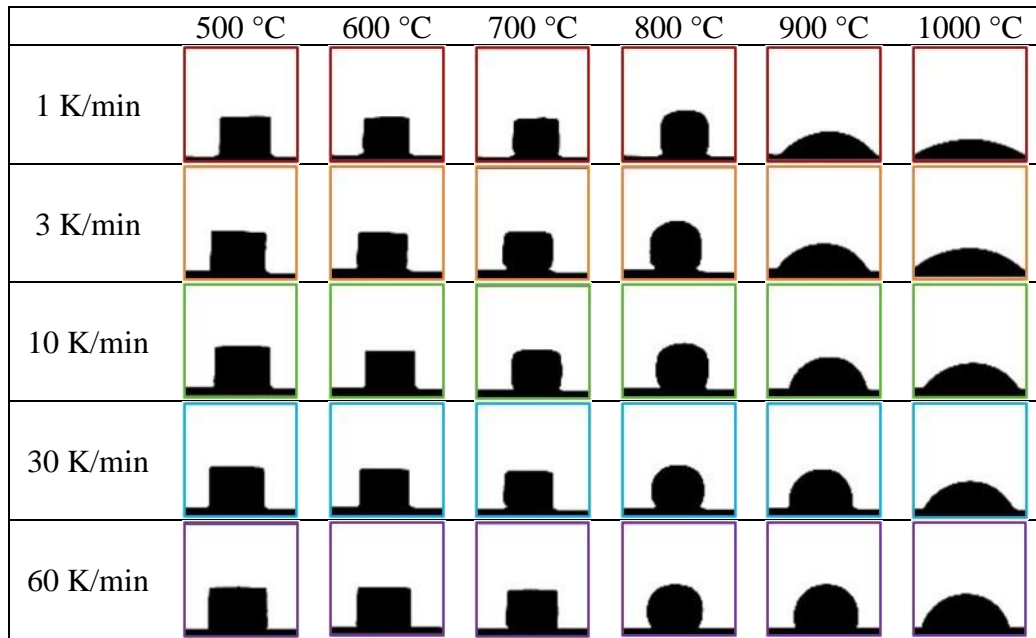
Figure 3. Silhouettes captured by HSM illustrating the morphology of glass frit compacts subjected to various heating rates.

BACKGROUND

A. Introduction to Sintering

1. Processes and Mechanisms

Sintering is the fusing or bonding of particles for powder consolidation, typically using heat, for the purpose of producing a coherent, densified body with controlled porosity, and in polycrystalline materials, grain size.[18] This consolidation is driven by the surface tension of the powder to extend the contact area between adjacent particles through material transport.[18-19] Sintering studies have gained momentum for the purpose of predicting microstructural evolution, and in turn material properties, as a function of variables such as temperature, time, particle size, initial density and applied stress.[2, 18] There are numerous sintering techniques, including but not limited to pressure assisted sintering, microwave sintering, spark plasma sintering, etc. Effectively, a material given enough energy will transport matter to produce a more energetically favorable system, in the context of lower energy surfaces of particles or grains. Sintering can occur via multiple mechanisms, including diffusion from the surface, lattice or grain boundary, vapor transport, and plastic flow.[19] For glasses, viscous flow is acknowledged to be the dominant transport mechanism responsible for sintering.[2-5, 18-20] Diffusion is proven to occur over longer time periods than the observed duration of glass sintering, and thus is of minor importance to viscous flow.[4]

Sintering is often sorted into three categories: solid-state sintering of crystalline materials (SSS), liquid phase sintering of crystalline materials (LPS) and solid-state sintering of amorphous materials – more commonly referred to as viscous sintering. [18] SSS and LPS have competing mechanisms that occur during sintering: *coarsening* or growth of grains or particles, and *densification* of powder compacts. Densification is shrinkage due to the reduction of pores, Therefore, examining shrinkage can be crucial in determining optimal sintering temperatures. Coarsening does not contribute to the porosity reduction of the compact, but is still considered a sintering mechanism since grain growth works to reduce surface energy. This grain growth can significantly influence the final microstructure of the material. SSS and LPS occur as atoms detach from a *source* and

diffuse towards a *sink*, and subsequently followed by an interfacial reaction where the atoms reattach to the sink; e.g., grain boundary diffusion, lattice diffusion, etc. Viscous flow, driven solely by the reduction of surface energy,[3] does not have a defined source or sink of matter,[18-19, 21] and its process is not based on diffusion.[4] Instead, amorphous materials densify as matter viscously flows without a true particle boundary. Thus, coarsening in the context of crystalline materials does not occur for amorphous materials. Bordia[18] cited several studies[2, 22-23] to suggest that unlike LPS and SSS, viscous flow is not influenced by geometrical factors like particle size and shape, as well as particle and pore size distributions. However, glass powder compacts of multiple particle sizes have shown dissimilar sintering behaviors.[21]

Sintering stages are often marked by the connectivity of the solid phase and its corresponding porosity.[18] These stages may overlap, but are commonly referred to as the initial, intermediate, and final stage. During the initial stage, adjacent particles form necks, which improves connectivity but narrowly increases density.[18-19, 24] The pores in the initial phase are interconnected and open. Considerable densification occurs during the intermediate phase. In the final sintering stage, the pores become isolated or closed and the solid phase is completely connected. Crystalline materials can experience significant grain growth during the final stage. The interaction between the pores and the grain boundaries controls the evolution of microstructure. Glasses are considered to sinter via a mass transport mechanism called viscous flow, where matter is transported on a macroscopic scale over the entire volume.[3-4, 18] Since there are no grain boundaries, there are no coarsening mechanisms, in the traditional sense, and no grain growth.[18] The three stages of sintering acknowledged by the glass sintering community are modeled by Frenkel[3] (the initial stage), Scherer[25] (the intermediate stage), and Mackenzie & Shuttleworth[4] (the final stage). The Scherer and Mackenzie-Shuttleworth models follow the Frenkel's energy balance principle. These classical models are the foundation for more recent analysis and theories that consider complicating factors such as particle size distribution, particle shape, and initial packing density.

B. Glass Sintering Stages and Classical Theories

1. Viscous Flow Definition and Initial Stage Sintering

Frenkel[3] was the first to propose that amorphous materials sinter by viscous flow. This theory states that the thermodynamic driving force for viscous flow arises from an energy balance concept where the rate of energy dissipated by viscous flow is equal to the rate of energy gained by surface area reduction. In other words, it is more energetically favorable for individual particles in a compact to coalesce by viscous flow to reduce the total surface area of the compact. When the material is provided enough energy (heat), a reduction in the viscosity of the glass, caused by an increase in temperature, will allow for the macroscopic flow of matter. Frenkel claimed the reciprocal of the viscosity coefficient must be connected with the self-diffusion coefficient. The self-diffusion coefficient, D, is proposed to be proportional to the reciprocal of viscosity, η, with the relation

$$\frac{1}{\eta} = \frac{D\delta}{kT} \tag{1}$$

where δ is the lattice constant, k is Boltzmann's constant and T is the temperature in K. While Frenkel's Theory about the driving force of initial stage viscous flow sintering is still widely recognized as true, the argument for diffusion has been dismissed because the time scale of diffusion is too great to describe the behavior that occurs during glass sintering.[4]

During the initial stage of sintering, the shared interface between particles grows rapidly. Therefore, it may be convenient to consider this stage in terms of the growth of this interparticle interface, or 'neck.' Necking is observed when two neighboring particles form a shared connection, like a bridge.[2, 5, 18-19, 21, 25] A schematic of the necking between two spherical particles is presented in Figure 4.
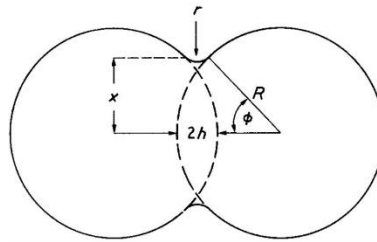
Figure 4. A geometrical model of two spherical particles coalescing to form a neck during the initial sintering phase.[2]

Kuczynski[5] was the first to propose the relation of neck growth with time:

$$\frac{x^2}{R} = \frac{3\gamma t}{2\eta}$$

(2)

where x is the neck diameter between two particles, R is the radius of the particles, γ is the surface energy, and η the viscosity.[5-6, 26-29] Clearly, this equation applies to isothermal sintering and assumes a monomodal particle size. Plotting the ratio of the square of neck diameter to the radius of the particle, x^2/R, as a function of time, t, a straight line with the slope $3\gamma/2\eta$ is obtained.[6] The value of surface energy, γ, has been taken to be 90 dyne/cm at the lowest viscosity values for sintering (i.e., when rapid sintering occurs) [27] and 313 dyne/cm for higher viscosities.[6] The mechanism responsible for neck growth has been investigated by observing linear shrinkage and assuming the rate of decrease of the center-to-center distance between two particles is linearly proportional to the linear shrinkage. [21] However, particle rearrangement is expected take place for randomly oriented powder compacts. The relative movement of particles may enhance shrinkage as particles move into larger voids, but anisotropic pore shrinkage may limit densification.[21, 30]

Geguzin[31] investigated the experimental effects of the true geometry of the contact area. The coalescence of amorphous materials was filmed to examine viscous flow that occurred solely due to surface tension forces. The meniscus at the contact of the spheres creates a compressive capillary force that pulls the centers together. Viscous deformation (shape change as a result of viscous flow) happens because of two combined pressures; (1) from the curvature of the neck and (2) from the curvature of the sphere surface. The ratio of these stresses is considered to be a function of sintering time. When the forces due to the neck curvature are much greater than the forces from the particle curvature, "viscous flow of material away from the straight line joining the centers occurs not only in the region of the concave portion of the neck surface but also in the regions adjoining convex portions of the sphere surfaces."[31] This is important because the concave parts of the surface generate a pressure that manifests itself beyond the immediate region of the concavity. It was concluded that this difference can significantly affect the initial stage of sintering.

Time is an important factor in these equations that has often been overlooked. German noted that sintering rate increases with lower viscosity (higher temperature).[26] This factor is the principal reason isothermal and non-isothermal sintering are not usually

comparable. German recalled the Arrhenius temperature dependent viscosity equation, valid over a limited temperature range,

$$\eta = \eta_0 \, exp\left(\frac{Q}{kT}\right) \tag{3}$$

where η_0 is a proportionality coefficient, Q is an activation energy, T is the absolute temperature, and k is Boltzmann's constant. The increase in temperature causes lower viscosity, thus increasing the rate of viscous flow and decreasing sintering time. Figure 5 shows sintering rate is a function of temperature. [26]
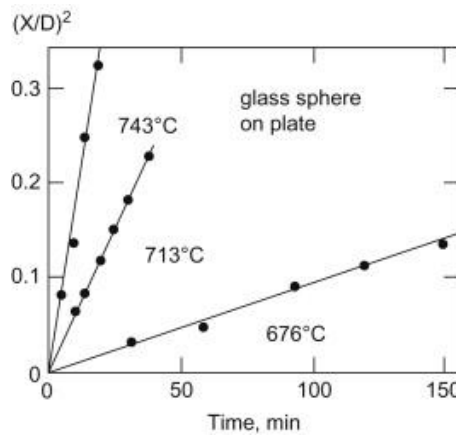
Figure 5. A plot of the square of the neck ratio (x/D), where D is sphere diameter, as a function of time to evaluate the glass sintering behavior at various temperatures. [5, 26]

While neck growth is significant during initial sintering, it is crucial to consider the elimination of porosity when discussing densification (and shrinkage). Zagar[20] proposed an isothermal densification model for viscous flow from a phenomenological view,

$$log\left(\frac{V_p}{V_{po}}\right) = \frac{-\gamma t}{2R\eta} \tag{4}$$

where V_{Po} is the total initial pore volume and V_P is the final porosity after sintering. It is important to note that pore size distribution affects densification due to the varying capillary forces that act on the particles. This stress will cause large pores to grow and small pores to shrink. [26,30] This is coarsening in a viscous matrix.[30]

Rabinovich[2] cited the rate of shrinkage that occurs during viscous flow as

$$\frac{\Delta V}{V_0} = \frac{3\Delta L}{L_0} = \frac{9\gamma}{4\eta R}t \tag{5}$$

9

Where ΔV is the change in volume, V_0 is the initial volume, ΔL is the change in length and L_0 is the initial length of the sample. Linear shrinkage has also been described by the relation [3, 23]

$$\frac{\Delta L}{L_0} = \frac{3\gamma}{8R\eta(T)}t \tag{6}$$

When the radius of the neck, r, grows to approximately half the radius of the particle, R, the intermediate stage of sintering commences, and the sintering rate is significantly reduced as sintering progresses.[19] Since amorphous materials do not have grain boundaries, the curvature of the neck will eventually reduce to zero, effectively removing much of the driving force behind the initial stage of viscous flow, thus challenging the theory that viscous flow is the sole mechanism fully densifying structures with low-packing density.[26]

2. Intermediate Stage

In the intermediate stage, the pore phase is still continuous, but it is assumed that the pore shape has reached equilibrium due to the surface and interfacial tensions.[19] Density of the sample increases up to 0.9 theoretical density presumably as a result of the shrinkage of pores until they eventually become unstable and close off creating isolated pores, at which point the material enters the final stage of sintering.

Scherer proposed a theory to describe the intermediate stages of viscous flow sintering when glass compacts still contain open, non-spherical pores.[25] To analyze this sintering behavior, Scherer visualized a cubic array of intersecting cylinders, as seen in Figure 6.
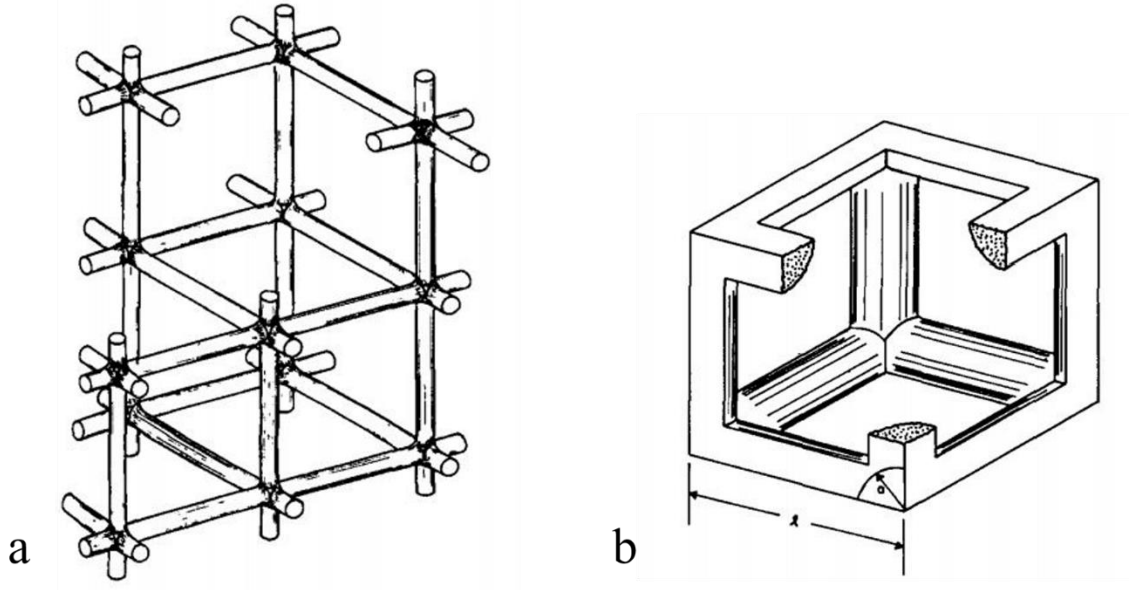
Figure 6. a) Scherer's model of intersecting cylinders and b) a "unit cell" of these cylinders of radius a and length l. [25]

The model simplifies the geometry while preserving the real material's integral features because the cylinders represent strings of oxide particles of the glass structure. The average particle size is represented by the cylinder radius, a, and the pore diameter, d, can be related to l, the length between two intersecting cylinders, when the cross-sectional area of the pore is equated to the void between the cylinders. Therefore, assuming

$$\frac{\pi d^2}{4} = (l - 2a)^2 \tag{7}$$

with pore size diameter data from mercury penetration and with an average particle size, one can calculate the ratio for a/l. The ratio of the length of a cylinder to its radius corresponds to the ratio of pore size to particle size, and the relation between a/l to relative density becomes

$$\frac{\rho}{\rho_s} = 3\pi \left(\frac{a}{l}\right)^2 - 8\sqrt{2}\left(\frac{a}{l}\right)^3 \tag{8}$$

where ρ is bulk density and ρ_s is the density of the solid phase (skeletal density). Plotting a/l as a function of ρ/ρ_s, there is reasonable agreement between measured values. This plot is shown in Figure 7.

$$\rho/\rho_s = 3\pi(a/l)^2 - 8\sqrt{2}(a/l)^3$$
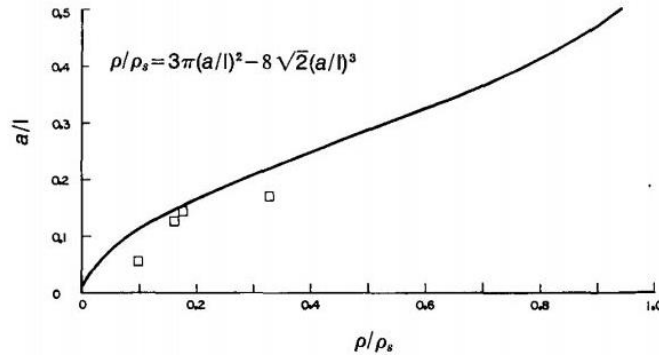
Figure 7. a/l as a function of ρ/ρ_s[25]

A different geometry for this model will not influence the shrinkage kinetics of the cylinders, but the densification rate will slightly differ depending on the relative amounts of solid phase included in the cylinders and corner sections. Rabinovich stated that the surface area difference between model and real material is approximately 35%.[2]

Scherer applied his model to experimental data by fitting densification data to obtain viscosity values. Reasonable agreement with beam bending viscometry data of fully sintered parts was observed. It should be noted that his model is intended for low density glasses with open porosity. [22] Scherer plotted relative density as a function of reduced time, Figure 8, for a silica soot preform and fitting the data to the theoretical curve, and observed a relatively good fit. Viscosity of different glasses was calculated using the sintering data and good agreement with real viscosity measurements was observed.
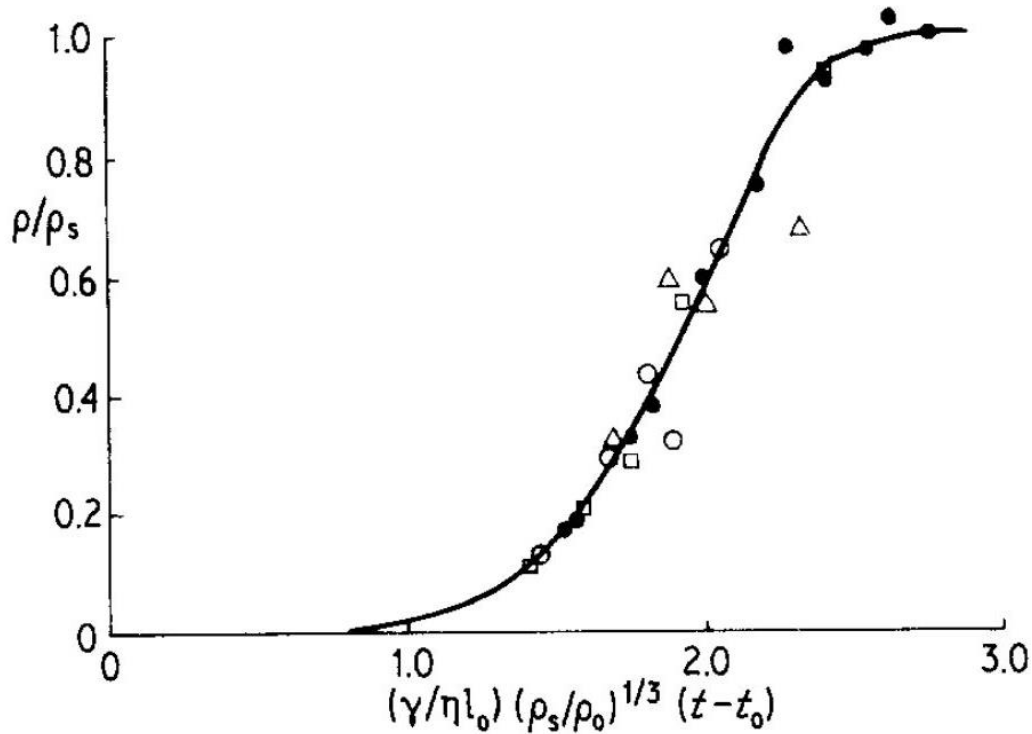
Figure 8. Relative density as a function of reduced time for a silica soot preform fired in air at 1115 °C (open circles), 1185 °C (closed circles), 1236 °C (squares) and 1327 °C (triangles), after Scherer and Bachmann. [2, 22]

Scherer's model breaks down at a theoretical density of 94%, when the cylinders run into each other. Theoretically this is the end of the intermediate sintering phase because the pores are closed.

3. Final Stage

A material is considered in the final stages of sintering when the solid phase is continuous and isolated pores are scattered about the microstructure.[19] Pores will continuously shrink and potentially disappear. This stage is best described by the Mackenzie-Shuttleworth model,[4] but their model should only be used when theoretical densities are greater than 0.94.[12]

The Mackenzie-Shuttleworth (MS) Theory is intended for uniform, rapid sintering of spherical monodispersed glass particles.[4] The model assumes all pores are isolated spheres of equal size randomly distributed throughout the solid material to simplify the calculations. The model also assumes the rate of densification is uniform throughout the body and rate of sintering is independent of the compact's size and geometry. It is proposed

13

that during viscous flow, the pore size will decrease but not disappear, therefore the number of pores should remain constant. It is noted that the pores do not necessarily have to be spherical to obtain a single densification rate, but the distribution of pore size and shape must be uniform throughout the entire compact.

Mackenzie and Shuttleworth identified at least two processes that transpire during sintering; 1) particles fuse together and pores evolve toward spherical and 2) density increases. While these processes occur simultaneously and are both driven by the surface energy of the powder exceeding that of the bulk, they may occur by separate mechanisms.[4] Mackenzie and Shuttleworth refuted the idea that the increase in density during glass sintering occurs through volume diffusion of vacant lattice sites or surface transport of atoms. It is claimed that these processes are too slow to account for the densification rates that are observed, and that mass transport must involve macroscopic flow, driven by surface tension. Diffusion may be involved in moving matter over short distances to change the pore shape, as atoms move from high-energy convex areas to lower-energy concave parts (which have greater inward pressure from surface tension) decreasing surface area and rounding the pores.

Mackenzie and Shuttleworth verified that Frenkel's theory is applicable to glasses but not metals since glasses have Newtonian viscosity while metal behaves like a Bingham *solid* during sintering. For a material to have Newtonian viscosity the rate of shear strain must be proportional to shear stress. Bingham solids have the rate of shear strain is proportional to the difference between the applied shear stress and a critical shear stress.[4]

The rate at which the radius of the pore, r_1, decreases when a pressure ($2\gamma/r_1$) is applied inside the pore can be calculated by setting energy dissipated by flow equal to the work done by surface tension. The process is treated as if it were steady state because the kinetic energy of the material is assumed to be negligibly small. Typical sintering experiments are conducted at a constant temperature measuring density over time. The volume of real material is constant, as is the number of pores (as long as all pores are equal in size). Relating relative density, ρ, and time, t, to number of pores per unit volume, n, surface energy, γ, and viscosity, η, with the volume of each pore as $4\pi r_1^3/3$ gives

$$r_1 = \left(\frac{3}{4\pi}\right)^{\frac{1}{3}} \cdot \frac{(1-\rho)^{\frac{1}{3}}}{\rho^{\frac{1}{3}}} \cdot \frac{1}{n^{\frac{1}{3}}} \tag{9}$$

Thus, the radius of the pores decreases as density increases.

As the British statistician George Box declared in 1976, "All models are wrong, but some are useful." Models are, by definition, a simplified representation of a system or phenomenon. The purpose of a model (or theory) is to provide a more intuitive explanation of a phenomenon, not necessarily to explicitly define it. Therefore, these models cannot precisely depict the exact kinetics of viscous flow sintering. Some of the limitations of these models are considered in the following section, not in condemnation, but in consideration that certain factors may be necessary to adjust the previous equations for the calculation of more accurate values.

C.   Limitations of Classical Models

1.   Non-isothermal Sintering

Classical theories assume sintering treatments occur isothermally, that is, at a fixed temperature. While this simplifies calculations, it does not accurately reflect real production in industry or typical sintering experiments, e.g., heating microscopy.

Cutler[32] examined the shrinkage of compacts consisting of 15-25 μm soda lime silicate (SLS) glass spheres with a PVA binder during heating rates of 0.46 to 2.91 K/min in an oxygen atmosphere with a water vapor partial pressure of 144 mm Hg. The shrinkage rates of compacts containing crushed SLS glass, screened to pass a 25 μm sieve, were also compared.

Cutler[32] extended Frenkel's theory for isothermal sintering of viscous liquids to propose an expression describing the non-isothermal heating of spherical glass compacts. He claimed that one may demonstrate temperature dependence of sintering and shrinkage simultaneously. Cutler cited Frenkel's shrinkage equation as

$$\frac{d\left(\frac{\Delta L}{L_0}\right)}{dt} = \frac{\gamma}{2a\eta} \tag{10}$$

Where a is the average particle radius, γ is the surface tension, $\Delta L/L_0$ is the (linear) fractional shrinkage, t is time, and η is viscosity. η corresponds to the viscosity-temperature relation of Equation 3 above, recognizing that Q (activation energy) and η_0 (or A, a proportionality coefficient) may gradually change with temperature. Temperature

increases linearly with time and constant heating rate, c, such that $T=ct$. These equations are combined to produce the relation of shrinkage at a constant heating rate.

$$\frac{d\left(\frac{\Delta L}{L_0}\right)}{dT} = \frac{\gamma}{2acA} exp\left(\frac{-Q}{RT}\right) \tag{11}$$

The slope, or integral, of the above equation is the change in shrinkage with respect to time at various temperatures and can be approximated as

$$\frac{\Delta L}{L_0} \approx \frac{\gamma RT^2}{2acAQ} exp\left(\frac{-Q}{RT}\right) \tag{12}$$

Over small temperature intervals γ and A are approximately independent of temperature. Differential shrinkage with respect to temperature, divided by the shrinkage, and multiplied by temperature squared, plotted against reciprocal temperature, multiplied by 1000, is proposed to yield a constant slope value of the activation energy divided by the gas constant, R, at each temperature.[32] Figure 9 is an example of this plot. A linear relation is observed for spherical particles. During high amounts of shrinkage, Cutler noted that the relation between temperature and shrinkage may deviate from linear, but this is not unexpected because sintering rate may be influenced by the method of compaction and the number of pores that would be associated with such large shrinkages. It is noted that irregular (crushed) particles would not show linear relations between shrinkage and time, in agreement with previous isothermal experiments.
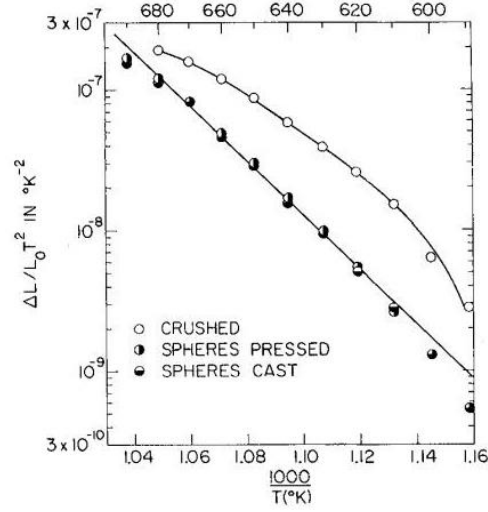
Figure 9. Shrinkage as a function of temperature for spherical and crushed glasses powders heated at 1 K/min. Note that the glasses are of different composition but of similar particle size. [32]

This technique is claimed to be more accurate than isothermal measurements when describing activation energy.[32] Cutler reports an activation energy range of 85 - 90 kcal/mol (356-377 kJ/mol). Isothermally treated samples will have a delay from the time it is inserted into the furnace to when viscous flow can actually occur to allow shrinkage; this technique eliminated that time delay.

Similarly, activation energy has been determined by comparing the temperatures at which equivalent shrinkages are observed for different heating rates.[32-36] Karamanov et al.[33] use an analytical technique based on the theory that viscous flow densification exhibits a linear shrinkage related to the activation energy for sintering, E_{sin}, by the equation

$$\frac{d\left(\frac{\Delta L}{L_0}\right)}{dt} = A_0 \, exp\left(\frac{-E_{sin}}{RT}\right) \tag{13}$$

Where $\Delta L/L_0$ is linear fractional shrinkage, t is time, R is the gas constant, T is absolute temperature, and A_0 is an Arrhenius pre-exponential factor at a constant particle size, for isothermal conditions. For non-isothermal conditions with a constant heating rate, υ, the equation above becomes

$$\frac{d\left(\frac{\Delta L}{L_0}\right)}{dT} = \frac{A_0}{\upsilon} exp\left(\frac{-E_{sin}}{RT}\right) \tag{14}$$

17

where υ is the heating rate. Karamanov et al.[33, 35] reference the Chen equation[34, 36] for the determination of activation energy, E, from linear heating rates as the integral of Eq. 14 giving

$$ln\left(\frac{\upsilon}{T_x^2}\right) = \frac{-E_{sin}}{RT_x} \tag{15}$$

Where T_x is the absolute temperature at which equal percentages of shrinkage occur. Karamanov et al. apply this equation to dilatometric data obtained using heating rates 5, 10 and 20 K/min to evaluate values of $E_{sin,}$ reporting a sintering activation energy for 10% shrinkage of 485 ± 15 kJ/mol for a waste ash glass and 245 ± 10 kJ/mol for a soda lime silicate glass.[33] Therefore, measuring shrinkage offers a practical way to evaluate sintering theory and determine the activation energy for sintering.

Panda and Raj[7] examined glass sintering using a various constant applied loads, comparing samples heated to 870 °C at 0.2 K/min and 920 °C at 2 K/min. Both heating profiles observed crystallization of the glass prior to peak temperature. The temperature at which maximum density was reached, also referred to as the inflection point, increased with heating rate, (856 °C for 0.2 K/min, 884 °C for 2 K/min), as seen in Figure 10.
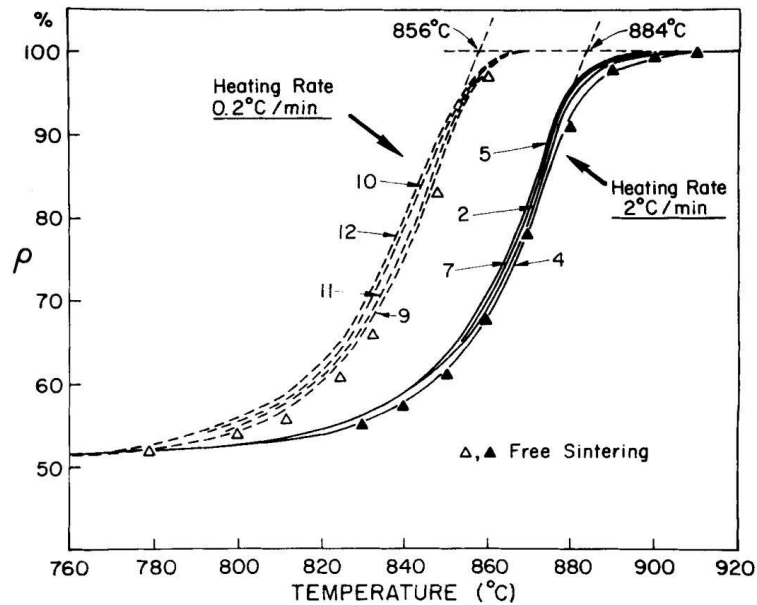
Figure 10. Density as a function of temperature for constant heating rates of 0.2 K/min and 2 K/min. Inflection points are the transition in densification rates to a plateau as the glass reaches theoretical density. Numbers along the curve refer to applied loads. [7]

18

Whether densification was terminated because it was complete or because of the onset of crystallization remained unresolved.[7] However, dissimilar heating rates are known to produce compacts of different densities due to partial devitrification. Low heating rates can allow surface crystallization glass particles, inhibiting further densification by viscous flow.[21]

2. Particle Shape and Size

The models mentioned above do not describe glass sintering universally but are simplified for the conceptual illustration of the mechanisms of material transport at work. A substantial limitation of these models is the assumption spherical monodispersed particles. While Bordia[18] presents arguments that viscous sintering is not influenced by geometrical factors, multiple studies have demonstrated effects of particle shape and distribution (which thus, affects pore size and distribution since pore size/distribution are inherited from particle size/distribution) on the sintering kinetics of glass powder.[21, 23, 37-49] Real particle shape and particle size distribution will influence sintering, especially the geometry near the neck contact,[40] as well as the mechanisms of material transport, the closure of pores (the rate of densification)[21, 37-38, 45] and the potential to devitrify before sintering is completed.[42, 47, 50-54]

It has been observed that jagged particles initially sinter faster than spherical particles.[41, 47-49] Cutler and Henrichsen[49] observed shrinkages as much as five times faster for jagged particles compared to spherical particles, as seen in Figure 11.
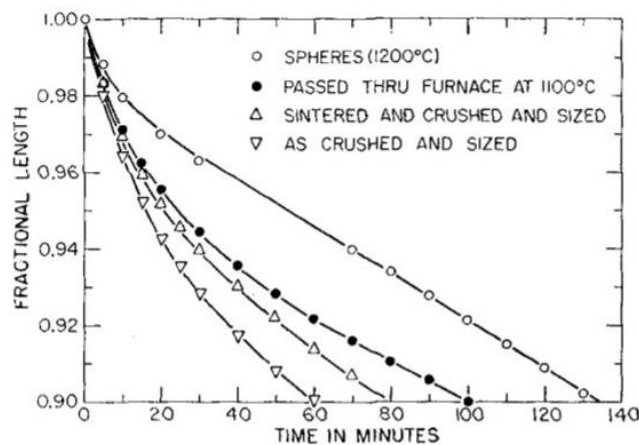
Figure 11. Various glass particle shapes with diameters 90 μm < d < 106 μm at 672 °C. Glass spheres were formed by dropping crushed glass through a heated tube (1200 °C). [49]

19

Frenkel's shrinkage equation, valid for the first 10% linear shrinkage, can be expanded to include a shape factor K_s

$$\frac{\Delta L}{L_0} = \frac{3\gamma K_s}{8\eta(T)r}t \qquad (16)$$

where ΔL is the change in length (or linear shrinkage) after some time t, L_0 is initial length of the sample, γ is the glass-vapor surface energy, K_s is a shape factor, $\eta(T)$ is the temperature-dependent shear viscosity and r is the initial particle radius.[47] K_s is taken to be 1 for spherical particles and up to 5 for jagged particles, but typically, K_s values vary from 1.8 to 3 and are generally used to fit the equation to measured values. Particle shape will affect the particle packing and pore size distribution, even for powders with the same particle size distribution, thus ultimately influencing the sintering kinetics. [51]

Petzow and Exner[55] examined particle rearrangement as a result of asymmetric neck formation from asymmetric stress of three 0.4 mm glass spheres. The formation of new contacts, differences in particle size, as well as any other effects that may cause non-uniform center-to-center approach, were referenced as contributing to stress. Contact formation is a function of the uniformity of packing and the packing density. It was concluded that atmosphere strongly affected the initial angles, where the angle is largest in an argon atmosphere, smaller in a wet atmosphere and even smaller in a dry atmosphere. This was attributed to the greater spreading of the deformation region around the contact over the particle surfaces when sintered in argon. Neighboring necks may interfere in the initial stages of sintering, indicating that the sintering atmosphere can affect the surface layer of particles and create a viscosity gradient from the bulk to the surface. Figure 12 depicts a model of particle morphology during sintering depending on their contact angle (left) and the increase in contacts of a particle as a function of neck radius squared when fired in argon, dry air and wet air (right). It appears that as the square of neck radius increases, the particles form more contacts in wet air.
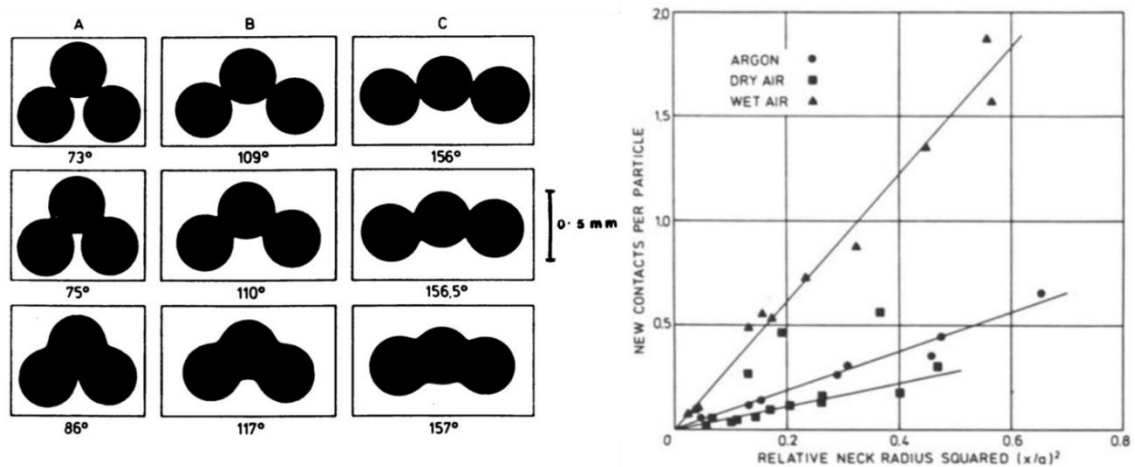
Figure 12. Particle models of glass spheres with different contact angles when sintered in argon (left) and average number of contacts per particle as new contacts are formed during sintering at 750 °C in various environments (right).[55]

Pore shape and size distribution, which is inherited from particle shape and size, will also affect sintering behavior. Shimohira et al.[21] used mercury porosimetry to compare the changes in pore size distribution as a function of various firing temperatures for amorphous silica spherical powders of a single particle size (monodispersed) and multiple particle sizes (polydispersed). Particle size distribution analysis was not investigated. Randomly oriented monodispersed powders were also compared to those that were close packed in a face center cubic (FCC) structure. Structures were verified by scanning electron microscopy (SEM). Randomly oriented monodispersed powders exhibited a bimodal pore size distribution (Figure 13a), while polydispersed powders exhibited a more normal pore size distribution (Figure 13b). A decrease in the mean pore size was observed with increasing firing temperature for monodispersed powders and an increase in mean pore size for polydispersed powders. Polydispersed spheres randomly oriented had the smallest average pore size and higher initial packing densities with the narrowest pore size distribution. However, upon heating, the average pore size increased, and the distribution skewed toward larger pores. The local pore growth was attributed to the stresses induced from varying particle size. It was supposed that both large and small particle sizes nearly equally contribute the same amount of material to the neck, and neck growth is inversely proportional to the shrinkage of the particle. As the center of the smaller sphere is drawn toward the center of the larger sphere, a void will grow on the side opposite to the neck contact point, which will induce a local stress if it is constrained. It was argued that pore

21

growth occurs at the voids near the smaller spheres since the larger spheres play a greater role in forming the particle network with necking links at contact points.
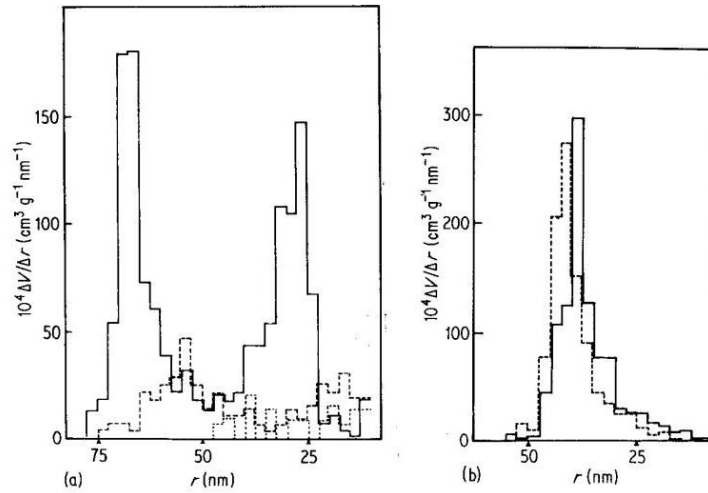
Figure 13. From[2], pore size distributions of a) monodispersed spheres of 0.3 μm where —— heated to 800°C, ---- 1000 °C ⋯ 1050 °C b) polydispersed spheres, —— heated to 600°C, --- heated to 800 °C.[21]

While real powder compacts will not exhibit FCC structures of monodispersed spheres, this experiment aids in the understanding of pore elimination phenomena that occurs during sintering by illustrating the two kinds of interparticle voids; smaller tetrahedral voids and larger octahedral voids. Particle rearrangement seems unlikely for FCC packing because of the 12-fold coordination and the neck formation connecting the particles together at each contact point to form a rigid network structure. Large pores tend to shrink before smaller pores. Shimohira concluded that mean pore size reduction is more favorable in compacts consisting of particles of the same size, and multiple particle sizes will increase the mean pore size due to the variability in decreasing center-to-center distances.

Sacks and Tseng[23] also investigated the effects of dissimilar pores on densification SiO_2 glass particles. Highly ordered compacts composed of 0.5 μm spherical particles were compared to compacts made from flocculated suspensions (0.5 μm spherical particles) and dispersed suspensions (0.35 μm spherical particles). Particle size did not appear to affect densification. However, ordered samples exhibited enhanced densification than samples prepared from flocculated suspensions, despite being subjected to the same thermal treatment. This discrepancy was attributed to ordered samples having uniform pore size

22

and more nearest neighbor contacts per particle. It was stated that reduced particle size does not necessarily increase densification rate because sintering kinetics are more dependent on the shape and distribution of the pores. This study concluded that pores of different sizes shrink at different rates and that smaller pores shrink faster than larger pores.

Prado et al. [51] emphasized an undescribed gap in viscous flow sintering when using in relative densities between 0.8 and 0.9; the Frenkel model is a valid description for initial sintering, but cannot be applied to densities greater than 0.8 while the Mackenzie-Shuttleworth model does not work for densities below 0.9.[47, 51] Prado et al. criticized one of the methods Scherer used to verify his model's applicability to compacts with pore size distributions.[51] Mercury intrusion porosimetry may provide misleading pore size distribution results because the fluid may penetrate the large pores by flowing through the small pores and because this method depends on the rate of pressure increase. To alleviate error that may arise from mercury intrusion porosimetry, hundreds of pores were measured via SEM and the volume fraction was mathematically determined using standard stereological calculations to determine pore size distribution.[51]

Giess et al.[48] observed that the Mackenzie-Shuttleworth model cannot accurately describe the final stage of sintering of polydispersed irregular cordierite glass particles, since small size particles sinter most rapidly and large particles may delay densification towards the end of sintering. The anisotropy in the ratio of axial to diametral shrinkage was the same, 0.7, for both spherical and jagged particles. Spherical particles, however, were observed to reduce the shrinkage rate.

Prado et al. [43-44] developed the Clusters model by to describe glass powder compact sintering of a particular particle size distribution. The model is based on the experimental evidence that small particles fill the voids between larger particles. An individual cluster of particles experiences the initial and final stages of sintering, as described by Frenkel and Mackenzie-Shuttleworth, respectively. Therefore, compact density is determined by the sum of the individual clusters, weighted by their volume fraction. A compact of pressed powder has an approximate relative density of 0.6 before heat treatment. The Frenkel model is valid for a relative density of nearly 0.8, above which the Cluster model uses the Mackenzie-Shuttleworth equation to calculate relative density of the cluster. Maximum experimental sintering rate coincides with this transition between models when the relative

density of a partially sintered compact is 0.8.[47] An SEM image of the cross-section of an alumino-borosilicate glass with a wide particle size distribution after 8% linear shrinkage, Figure 14, suggests that the Frenkel model and the Mackenzie-Shuttleworth model may overlap, occurring simultaneously in polydispersed samples. [51]
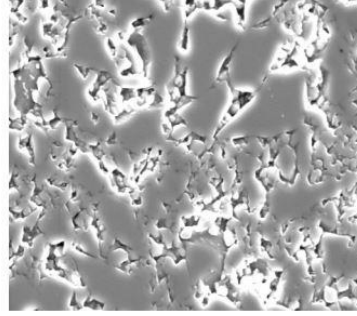
Figure 14. SEM of polydispersed alumino-borosilicate powder compact partially sintered illustrating the microstructure after 8% linear shrinkage, width of image is 20 μm. [51]

Considering that smaller particles will preferentially cluster in the voids of larger particles and sinter more rapidly, smaller clusters may reach the final sintering stage while large particles are still in the initial sintering stage. Thus, the sintering kinetics for real materials is more complex than the classical models imply. However, classical models still function as a foundation for more complicated theories with non-isothermal sintering and a particle shape and size distribution.

D. Viscosity and the Glass Transition

1. Introduction to Glass Viscosity

Viscosity is the resistance of a liquid to shear deformation with time, or the ratio between the applied shearing force and the rate of flow of the liquid.[56-59] Viscosity can also be thought of as the inverse of fluidity. The relation between the viscosity, η, and a force, F (i.e., the shear or deformation force) is expressed by

$$\eta = \frac{Fd}{Av} \qquad (17)$$

Where A is the area of two parallel planes separated by a distance, d, and v is the relative velocity of a fluid between the two planes. A liquid is said to behave as a Newtonian liquid if the viscosity is independent of force and the velocity varies directly with the applied shear force.[56] If the viscosity of a liquid is a function of the shear deformation rate it is said

to have non-Newtonian behavior. Most glasses behave as Newtonian liquids. With constant volume, change in shape due to a shearing force is the shear viscosity.

Viscosity can be presented in two different ways; as an experimentally measured viscosity at a given temperature (isothermal viscosity) or as an isokom temperature which reports a temperature for a given viscosity, such as T_g.[56] Viscosities of glasses fluctuate with temperature over an exceptionally wide range, where reference viscosities alone range over 12 orders of magnitude. Several specific isothermal viscosities and isokom temperatures are depicted in Figure 15. Since the span of glass viscosities is so large, there is not a single technique capable of measuring the range. Instead, multiple techniques are used to measure viscosities over particular intervals and combined to make up the entire spread. Most commonly used viscometers for glass are fiber elongation, which measures viscosities from 10^5-$10^{15.5}$ Pa s, beam bending viscometry (10^7-10^{12} Pa s) and rotational viscometers such as parallel plate (10^5-10^9 Pa s).[57] For very fluid melts, falling sphere viscometers can be used to measure viscosities between $10^0 < \eta < 10^6$ Pa s.[56] Figure 15 is a typical viscosity-temperature plot for a soda-lime-silicate glass depicting the appropriate viscosity ranges over which these techniques can be applied.
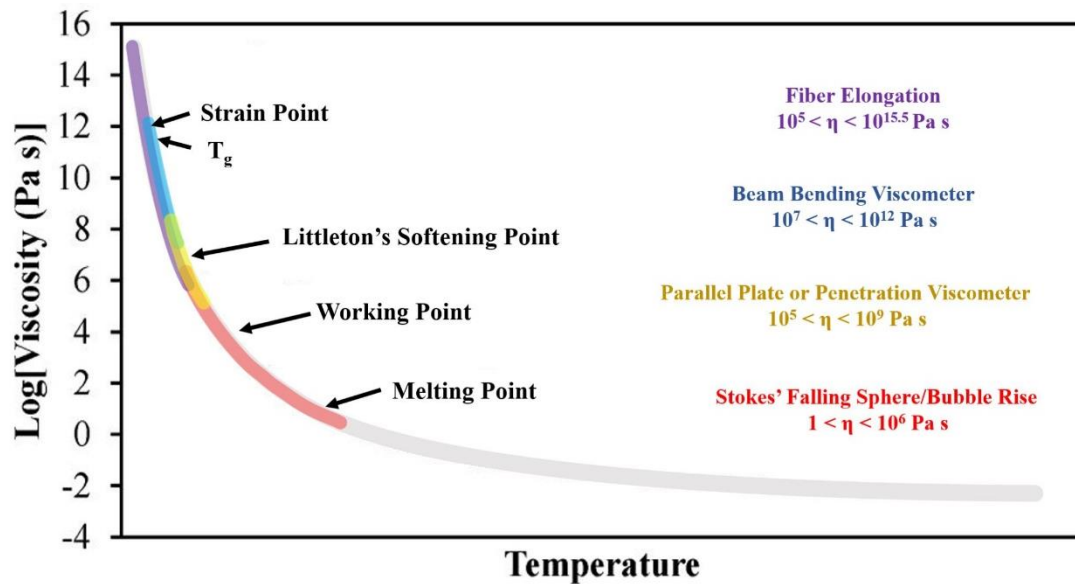
Figure 15. A general viscosity versus temperature curve for a soda lime silicate melt with reference viscosity points and several viscosity measurement techniques for measuring different ranges of viscosity. Reproduced from Zheng and Mauro.[57]

There are several reference temperatures that are important to know when working with a glass and five of these reference temperatures are pointed out in Figure 15 at the

corresponding viscosities which define the temperatures at which such points occur. Throughout the forming process, industry requires particularly precise control of the glass viscosity to generate sufficient throughput for quality, replicable product yields.[56] The 'melting point' is not truly the temperature at which the solid crystal exhibits a phase transition to a liquid, but the practical melting temperatures at which glasses are typically melted in industry where the viscosity is fluid enough that it meets the needs of production, e.g. the removal of bubbles (fining). This practical melting temperature occurs at viscosities approximately 10^0-10^1 Pa s. Once the melt is homogeneous and fined, it can be formed at slightly higher viscosities where it is viscous enough to retain its shape after forming but still fluid enough to move under reasonable forces. This is often referred to as the 'working point' which defined to occur at a viscosity of 10^3 Pa s. After forming, the object must be supported until the viscosity reaches Littleton's softening point, $10^{6.6}$ Pa s, where it will not deform under its own weight. The working range is the temperature range between the working point and the softening point, in which glass formers may still shape the piece using sufficient stress. The dilatometric softening point, T_d, (or in some cases T_{soft}) is not included on the viscosity-temperature plot as it is not exactly a viscosity specific temperature. T_d can occur at wider viscosity ranges than other characteristic temperatures and is reported to occur in a viscosity range of 10^8-10^{10} Pa s.[56, 58] T_d is important when considering thermal expansion, and thus can be obtained during dilatometry as the temperature at which the glass sample reaches its maximum length during heating, as demonstrated in Figure 16.
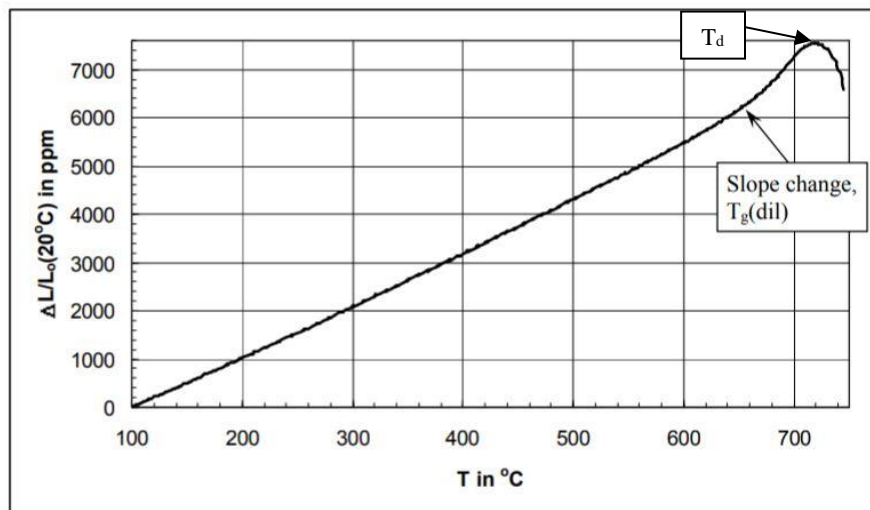
Figure 16. Relative length change of a material as a function of temperature example. [60]

At the annealing point, which occurs at a viscosity of 10^{12}-$10^{12.4}$ Pa s, internal stresses that result from cooling are relieved in minutes. At the strain point ($10^{13.5}$ Pa s) stresses are relieved in several hours. Glass transformation temperature, more appropriately referred to as the glass transition range, have average viscosity of $10^{11.3}$ Pa s for common glasses, according to Moynihan.[61] However, this range is often recognized as occurring at viscosities of 10^{12} Pa s.[56] Glass sintering viscosity is proposed to occur between the glass transition temperature and the softening temperature. [8-9]

The viscosity of a glass is closely related to the connectivity of the structure. The connectivity depends on composition, as well as temperature and thermal history. Generally, when a composition has reduced connectivity, it will also exhibit reduced viscosity, and vice versa. For example, as more alkali oxides or other network modifiers are added to a silicate melt, the connectivity will decrease resulting in a viscosity decrease. This means T_g and other isokom temperatures will decrease; the structure has more configurational flexibility and will break up and 'melt' into a liquid at lower temperatures.[56] Adding alkali to a silicate glass generally lowers the viscosity at a given temperature as a result of a less connected network. However, if compositions contain two or more alkali oxides, viscosities are lower than those of compositions with the same molar concentration of alkali if only one is present.[10, 56] This anomalous phenomenon is known as the mixed alkali effect, and is most evident at low temperatures. The boron anomaly will also affect viscosity temperature relation in alkali borate melts when plotting viscosity as a function of alkali content. [58] There are pronounced maxima in these plots at low temperatures, the magnitude of which tends to reduce with increasing temperatures. Kuppinger and Shelby[62] suggested that viscosity increases as a result of an increase in non-bridging oxygens when 3-coordination planar boroxol groups transform to 4-coordination 3-D tetraborate groups.

It is clear that glass viscosity is a function of temperature as well as composition or connectivity of the structure. Thermal history is not expected to influence glass viscosity in this study since all experiments were conducted on pre-melted glass powders. Additionally, the compacts are heated through the annealing temperatures during heat treatment, relieving any stress that may have arisen during initial melting and cooling preparations.

2. Glass Transition

a. Definition

T_g is the temperature at which certain temperature dependent properties of a glass melt initially deviate from the behavior of a supercooled liquid during cooling.[63] Macroscopic properties of liquids, such as enthalpy or volume, can change as a function of temperature (at constant pressure) instantaneously as the configuration of the liquid changes.[61] Figure 17 displays a typical enthalpy versus temperature plot of a glass melt cooling from its liquid state to absolute temperature. If the system cools quickly, the liquid will not be able to equilibrate allowing atoms to organize into an ordered structure. The temperature at which deviation from the supercooled equilibrium line occurs is dependent on cooling rate. For extremely fast cooling rates, the initial departure from the supercooled equilibrium line will occur at higher temperatures, whereas slower cooling rates will result in a deviation at lower temperatures. Thus, different cooling rates will also result in different changes in enthalpy or volume. Therefore, the glass transition temperature is more accurately described as a temperature range in which the glass deviates from equilibrium.

The plot in Figure 17 is divided into three different regions to define the ranges of (1) equilibrium liquids, (2) supercooled liquids and (3) glasses.[64] Equilibrium liquids are thermodynamically stable liquids above T_m and will never crystallize. Supercooled liquids are metastable liquids existing between T_m and T_g that will eventually crystallize after sufficient time. Glass structures are observed via experiment and molecular simulation to have similar structures to the supercooled liquid parents from which they cool. [64] Glasses are nonequilibrium solids existing below T_g that will flow under the action of gravity and spontaneously relax toward the supercooled liquid state if subjected to sufficiently long thermal treatments or in infinite time. They will first relax toward the supercooled liquid, and then toward a crystal where the flow will eventually stop as the material devitrifies becoming a true solid with a crystalline structure. However, the time scale at which these processes happen at ambient temperatures is beyond that which can be observed. The glass transition is defined as the temperature where the average time for the structural relaxation of the supercooled liquid, τ_R, is comparable to the observation time, t_{obs}. When a glass is heated, it will become a supercooled liquid at T_g. Additionally, there is a final "ultimate" region of this diagram; crystals are thermodynamically stable true solids made up of atomic

structures with long range order. The ultimate fate of a supercooled liquid or a glass is to crystallize, but the time scale can range from minutes to millennia. [64]
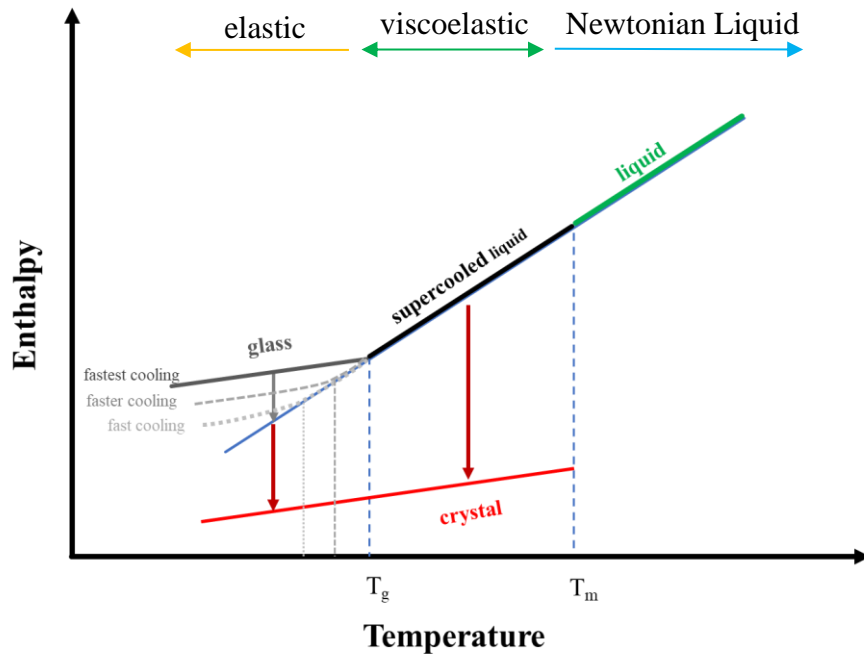
Figure 17. Typical schematic plotting enthalpy as a function of temperature for glass forming systems and the four states a glass may take: liquid, supercooled liquid, glass, and crystal. Abrupt change in slope at T_g depends on cooling rate. Reproduced from Zanotto and Mauro.[64]

b. Measuring T_g

T_g indicates a transition in thermo-mechanical properties of a material from viscous to elastic, such as a change in thermal expansion or the onset of viscoelastic behavior.[56-57] Thus, T_g is determined by analyzing the temperature dependence of a property, such as measuring how volume (or sample length) or heat capacity changes with temperature. However, these measurement techniques are reported to determine 'radically' different quantities for T_g.[65] The coefficient of thermal expansion (CTE) is the temperature coefficient of the length of the sample, while heat capacity is the temperature coefficient of the enthalpy of the sample. The relation between temperature and sample length or enthalpy is termed an integral dependency, while CTE and heat capacity differentially depend on temperature. Thus, T_g can be determined from either differential or integral dependencies of a property, but corresponding T_g values will differ.

Dilatometry is used to determine the coefficient of thermal expansion, by measuring the change in volume as a function of temperature.[56] Plotting relative length

29

change ($\Delta L/L_0$) as a function of temperature, CTE is the average slope over a certain temperature interval, ΔT.[60] The thermal expansion curve will experience a variation at the glass transition temperature, and, therefore, dilatometers can also provide a value for T_g. A pushrod dilatometer uses a linear variable differential transducer (LVDT).[58] A monolithic sample with flat parallel ends is placed between two pushrods in a furnace. The pushrods measure the expansion or contraction of the material as a function of temperature. At the onset of the glass transition range, there is a rapid rise in expansion. As temperature increases, the expansion curve hooks downward, as seen in Figure 16, due to the softening of the sample causing the penetration of the pushrods into the material or the sample sags with gravity as the viscosity reaches about 10^9-10^{10} Pa.s. This is the dilatometric softening point, T_d.

Any measurement of T_g is composition dependent, but may also be influenced by heating rate (and cooling rate when measuring enthalpy and heat capacity) and thermal history (fictive temperature) of the glass.[56, 61] Faster heating rates can cause an increase in apparent glass transition temperature. A heating rate of 5 K/min is recommended for dilatometric measurement of T_g.[65] Additionally, the pressures exerted on the dilatometric sample by the push rods will affect T_g such that higher pressures decrease the apparent measured glass transition temperatures. Optical dilatometers can avoid this pressure effect (neglecting the force of gravity). Optical dilatometers are contactless and have the potential to not only measure glass transition point, but also fictive temperature and activation energy of viscous flow of pressed powder samples, according to Karamanov et al.[35] The optical dilatometer measures the thermal expansion of the sample with two high definition cameras a capturing the tips of the sample. Optical dilatometers are claimed to have considerably higher accuracy than similar measurements from heating microscopy because of the camera quality. It is claimed that samples exhibiting fully viscous behavior can be observed with this technique, allowing one to study the kinetics of sintering process driven by viscous flow and the influence of crystallization on densification. [35]

3. Viscosity-Temperature Relation and Models

The viscosity-temperature relation is perhaps the most important plot in the glass community. There are several specific viscosities on a viscosity temperature curve that are

used as reference points, as seen in Figure 15, because of their practical relevance in processing and forming glass.[56] These viscosities are generally composition independent, and are often referred to by their corresponding temperature, which *is* composition dependent. An example of this is the glass transition temperature, T_g, which occurs for most glasses at roughly 10^{12} Pa s, but the actual temperatures can range hundreds of degrees depending on the structure and stability of the glass network.

The temperature dependence of viscosity is often expressed using the Arrhenian equation

$$\eta = \eta_0 e^{\Delta H \eta / RT} \tag{18}$$

where η_0 is a constant, ΔH_η is the activation energy for viscous flow, R is the gas constant, and T is the absolute temperature. This is essentially equivalent to Eq. 3. Glass-forming melts typically exhibit Arrhenian behavior at low viscosities ($< 10^3$ Pa s), but also within the glass transition region of 10^{13} to 10^9 Pa s.[56] However, the temperature dependence of viscosity between these two regions is considered non-Arrhenian because the activation energy for viscous flow is much lower for a fluid melt compared to that in the transition region.

The Vogel-Fulcher-Tammann, or VFT, model, developed by three investigators independently at approximately the same time in history, used three fitting parameters to accurately predict viscosities over 10 orders of magnitude.[57] Fulcher[66] was the first to publish his proposed equation in 1925, which modified the Arrhenian expression with a fitting parameter, T_0, to account for the variability of the activation energy for viscous flow, and replaced ΔH_η with a less defined variable, B and η_0 by a constant A.[56] The logarithm of this modified Arrhenian equation is

$$\log \eta(T) = A + \frac{B}{T - T_0} \tag{19}$$

Where A, B, and T_0 are the fitting parameters. The VFT model will overpredict viscosity at low temperatures as the curve diverges at finite temperatures, $T = T_0$. This means the equation implicitly, and physically incorrectly, assumes that there is no configurational entropy at a finite temperature. Since it was based on viscosity analysis of silicate glasses, Fulcher's model works well for oxide glasses but breaks down when applied to more fragile

glasses.[57] Vogel and Tammann individually developed mathematically similar equations to predict viscosity.

E.   Heating Microscopy

1.   Origin and Capabilities

The observation of a sample during thermal treatment aids in the understanding of material behavior during processing and has been around since the discovery of fire when man first watched wood burn. Heating microscopes have become very popular in materials science due to their broad range of application, especially in traditional and advanced ceramic and glass industries, power plants and metallurgy. [17] The behavior during heat treatment of glazes, glasses, ashes, coals, slags, and more can be directly characterized using a heating microscope.

The heating microscope can be used to analyze the densification, sintering crystallization, and melting behaviors of materials. Direct observation of the sample permits comprehensive analysis during typical industrial firing cycles. The microscopes generally magnify up to 10x, effectively capturing macroscopic shape and dimensional changes in the range of tens of microns to millimeters, yet it is conventionally termed "heating microscopy."[63]

Heating microscopes were commercially introduced in the 1950s,[17] but required manual observation, which was not only tedious but results were subjective and often limited to determining only the 'softening temperature.' Rapid heating rates were also unattainable. The technology to accurately, quickly, and reproducibly observe and quantify the sample evolution has since been improved. Today, computer software objectively measures height, width, and wetting angle. A heating microscope observes the deformation and shape evolution of a powder compact as a function of temperature. The information recorded by this instrument is of substantial practical significance; not only characterizing the material, but may also solve technological issues and manufacturing difficulties observed in glass and ceramic industries.[15] Heating microscopes can measure necessary material characteristics that can help manufacturers determine conditions, boundaries and thresholds for various processes. The instrument can reach temperatures up to 1600 °C at

heating rates as fast as 80 K/min. Rapid heating rates are relevant in industry since some kilns are constantly held at temperature and samples are inserted from room temperature. The instrument is also capable of implementing a dwell time, where the furnace will remain at a constant temperature for a specified time. Images of the sample are acquired at predetermined time or temperature intervals during the heating cycle and dimensional parameters are automatically measured. Characteristic temperatures are provided during the test as the sample progresses through each stage from initial shrinkage to the flowing of the melt. The sample size is relatively small (approximately 3 mm x 2 mm) which ideally reduces the influence of a thermal gradient and the difference between the temperature recorded by the thermocouple and the temperature of the sample. The test method has been found to be quite reliable, with a narrow range of variation. [17] The geometrical dimensions are specifically selected to balance the forces of gravity, viscous flow and surface tension during the heating and melting process. The microscope focuses on a plane that does not change during the shape evolution and a cylindrical shape is the only shape that allows this. Prism samples would require continuous manual refocusing of the camera.

Heating microscopes observe shape morphology of a pressed powder compact as a function of temperature and heating rate (time). Characteristic temperatures were defined in the German DIN 51730 regarding the fusibility of ash for fuel testing published in 1954.[17] The equivalent standards are ASTM D1857 and ISO 540. The hot-stage microscope (HSM, Misura ODHT, Expert System Solutions version 3.32, 32-bit system, Modena, Italy) is engineered to follow these standards.

In the HSM, a cylindrical sample is placed on an alumina support atop a Pt/Rh thermocouple in a small electric furnace (100 mm long, 20 mm diameter) between a light source, (halogen lamp) and a quartz or sapphire window, behind which a 5x magnification observation unit (camera) and recording facility are stationed. [17, 47] The camera detects the silhouette of the compact and computer software records precise dimensional changes using pixels (accurate to the nearest 10 μm). Shrinkage rates may easily be calculated from these measurements. Figure 18 is an example of the image captured by the HSM, highlighting the height and width of the sample. [17] Computer software considers characteristic sample shapes when determining temperatures for sintering, softening, melting, and flowing, as seen in the appendix. [17] Several of these shapes are based on ratios

of the width and the height. It should be noted that the resulting temperatures are sure to be dependent on heating rate.
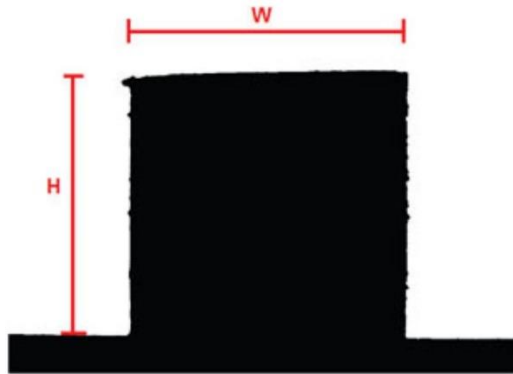
Figure 18. The silhouette of a cylindrical sample in the HSM. Software measures the changes in the width, w, and the height, h. The bottom section not included in the height range is the alumina support. [17]

A typical plot of sintering percent (height variation with respect to its initial size) as a function of temperature is shown in Figure 19. In this figure, the behavior of a glass frit sample that does not crystallize during heating is compared to one that does. The sintering plateau, where the sample dimensions are constant for an interval of temperature, marks the maximum shrinkage achieved via sintering. The temperature continues to increase and the viscosity decreases exponentially, but the surface tension does not change until the softening point. As temperature continues to increase above softening, the glass behaves like a liquid, surface tension decreases, the sample evolves to a sphere, then a hemisphere until finally melting is realized. The crystallizing frit exhibits a long sintering plateau as a result of crystal nucleation and growth within the sample. While the information provided by sintering percent as a function of temperature (Figure 19) is helpful in determining shrinkage in the vertical direction (linear shrinkage of the height of the sample), it does not consider shrinkage in the axial direction. Area variance considers the total change in area of the captured image, reporting shrinkages in all directions. Thus, the data analyzed in this study is strictly based on the area variance as a function of temperature.
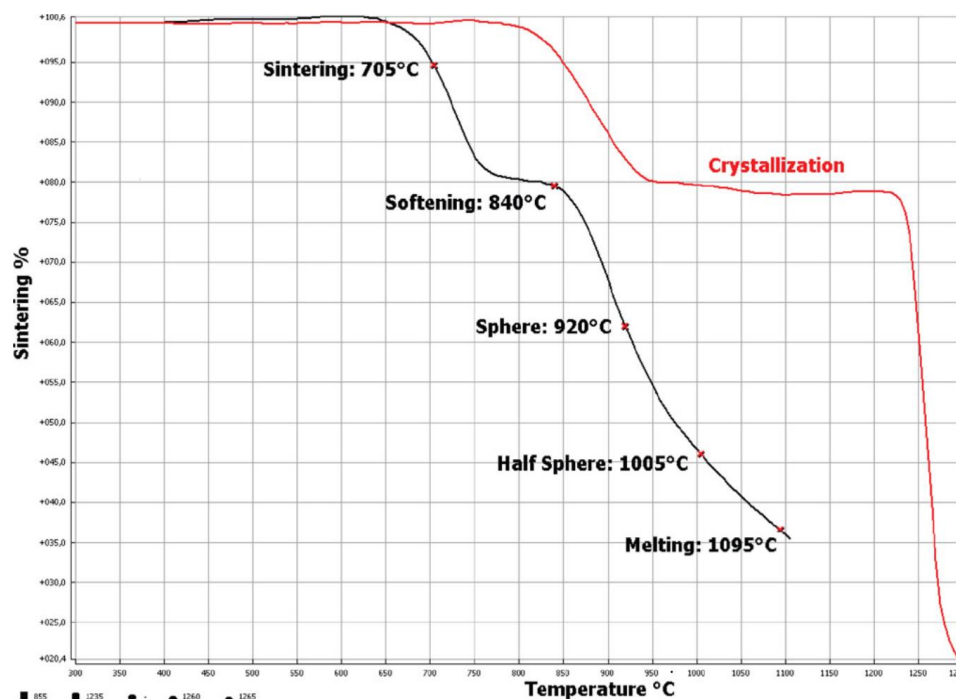
Figure 19. A typical sintering percent as a function of temperature plot for a glass frit with no devitrification behavior, and a frit that crystallizes during heating. Characteristic temperatures are identified along the vitreous specimen.[17]

The software is programed to provide a "sintering temperature" when the sample height decreases to some extent. The manual suggests that "sintering temperature" occur when the height of the sample decreases to 95% of the original sample, but may be adjusted by the user. However, this technique is limited because it is solely based on shrinkage which is largely influenced by particle packing and dissimilarly packed frits will shrink at different rates.[21]

It has been claimed that the HSM apparatus may have the capability of optical dilatometry.[67] Optical dilatometers are limited to a resolution of no less than 0.1 μm as a consequence of the wavelength of light, but the HSM has been shown to provide reproducible results within 1 μm. While this resolution is substandard, the data collected by this technique is very useful when observing the linear shrinkage that occurs during sintering.[67]

Scholze[11] is recognized as the first to use a heated microscope to correlate characteristic geometries of a cylindrical sample during heating to viscosity measurements. Pascual et al.[12] expanded on Scholze's work to propose a method using a heating microscope to determine glass viscosities at characteristic points, including the

35

temperatures where first shrinkage (Frenkel regime) and final shrinkage (Mackenzie-Shuttleworth regime) occur.

2. Characteristic Shapes and Corresponding Viscosities

Scholze[11] approximated the viscosities of the characteristic shape morphologies of the sample as a function of temperature by comparing the observed temperatures of these shapes to a viscosity-temperature curve produced from high temperature viscometer measurements. Scholze follows standard DIN 51 730, which marks various characteristic shape geometries and relative heights observed during heating in a microscope, including, first shrinkage, softening, hemisphere, and flow point. The sintering zone is evaluated according to images that capture the sample height (Figure 20a), but the main reaction zone of the melts is separated by two inflection points in the percent height as a function of temperature plot (Figure 20b). It is noted that the choice or a particular condition as a measured variable only has meaning if it is easily identifiable. For instance, the hemisphere point is easily identified by shape but some other characteristic points commonly encounter difficulties in identification. However, for sintering, the area of the sample (height and width) may change without compromising the contours of the shape, as opposed to softening when the edges of the sample start to round. The transitions occurring in the softening range evolve slowly and are not as sharply identified, introducing some uncertainty in the measurements of temperature. Therein lies the qualitative versus quantitative argument of the methodology and measurement capability available in 1962; today's software measure pixels providing more accurate and repeatable data. Scholze proposed that the characteristic points of nine observed glasses occur at the same viscosity, regardless of composition. The deformation point, or the sintering point, is distinguished from the softening point when the sample begins to widen, (within the accuracy of 20 degrees). He concluded that surface tension may influence the width of the minimum baseline, but otherwise has no observable effect on the viscosity. It is stated that viscosity differences had a variance up to 20%, which is still acceptable because that corresponds to a temperature difference of only 5 degrees. For faster heating rates, it is speculated that characteristic shapes are manifested at higher temperatures and correspondingly lower viscosities.
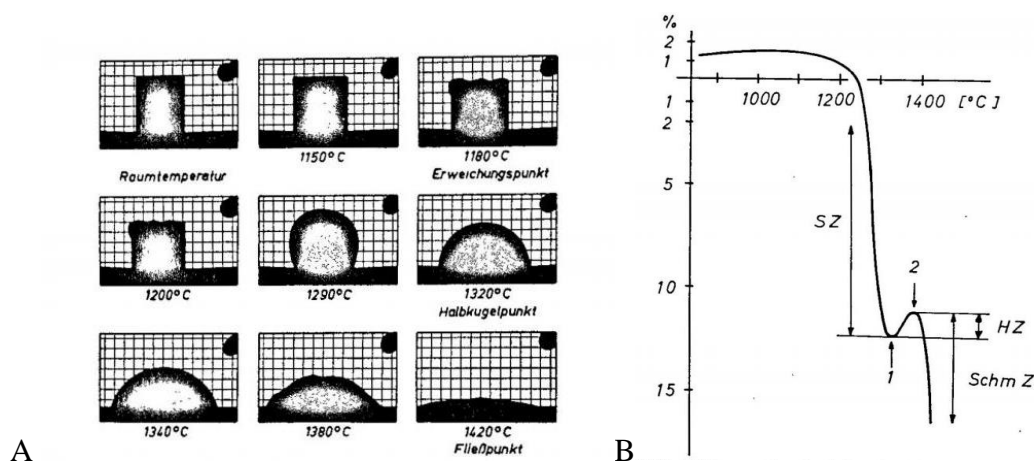
Figure 20. A) Characteristic shapes observed during heating and B) Linear shrinkage as a function of temperature, the main reaction zone is designated as between the two inflection points.[11]

Scholze determined characteristic viscosities of silicate glasses using a heating microscope and established a relation between conventional viscometry data in the viscosity range 10^9 -10^2 Pa·s.[*] Determined viscosity points including the transformation point (10^{12} Pa·s) the Littleton point ($10^{6.6}$ Pa·s) and the 'sinking' (potentially flow) point ($10^{3.22}$ -$10^{3.31}$ Pa·s) were used to calculate the constants of the VFT equation. Powder compacts comprising of particles < 75 μm were placed on an alumina support and heated at 7 K/min in a high temperature Leitz Wetzlar hot-stage microscope.[8] Scholze applied the temperature data from the photomicrographs correlated to the geometrically defined points from DIN 51730 to the VFT equation for each composition to calculate the viscosities at these temperatures.[8] Scholze defined the characteristic points first shrinkage (10^9 Pa·s) where the height first starts to decrease, maximum shrinkage ($10^{7.2\pm0.5}$ Pa·s) where the sample has decreased in size as much as possible before it begins to soften, softening ($10^{5.1\pm0.2}$ Pa·s) the rounding of edges first begins, half ball ($10^{3.6\pm0.1}$ Pa·s) where the silhouetted image evolves into a semicircle, and flow ($10^{3.1\pm0.1}$ Pa·s), where the maximum height of the molten glass reaches a specific unit on the microscope scale.[8] Scholze concluded that the characteristic points determined by the photomicrograph images occur in narrow viscosity windows, regardless of composition.[8] Similarly, Schlim et al. proposed that initial sintering begins at a viscosity 10^9 Pa·s, ends when the viscosity reaches 10^7 Pa·s, and the softening point occurs at viscosity $10^{5.5}$ Pa·s.[13]

---

[*] Viscosities were reported in Poise and converted to Pa·s

Pascual et al.[8] criticized the limited definition of the VFT curve in Scholze's work. Scholze adopted only three conventional viscosity points to adjust the VFT curve and lacks viscosity data below $10^{3.2}$ Pa·s.[11] Following Scholze's proposed method, Pascual et al.[8] incorporated experimentally measured data produced from high temperature viscometers to present a more complete viscosity-temperature curve for E-glass, Pyrex, SLS, and two in-house borosilicate glasses, one of which was expected to exhibit the mixed alkali effect. The error in viscosity intervals of the characteristic points in silicate glasses was also assessed. Fiber elongation was used to measure viscosity intervals between 10^{13}-10^8 Pa·s and rotation methods were used to measure viscosities of melted glass ranging from 10^5-10^1 Pa·s, providing 15 experimentally derived data points to adjust the VFT equation for a more defined viscosity-temperature curve with regression coefficients of r^2>0.9999. Only viscosities below 10^{12} Pa·s were included as to avoid the relaxation phenomena. Glass compacts 3 mm tall with particle size between 12-20 μm were placed on an alumina support and heated at 5 K/min in a Leitz Wetzlar hot-stage microscope. The photomicrographs of shape evolution at temperatures, as defined by Scholze - first shrinkage, maximum shrinkage, softening, half ball, and flow - were analyzed corresponding to the characteristic viscosity points. Viscosity temperature curves between 550-1500 °C were studied, and as expected from a range of silicate and borosilicate compositions, the glasses exhibit substantial viscosity differences as well as the dependence of viscosity on temperature.

The log η values for each of the viscosity points can be obtained by substituting the temperatures for each characteristic point in the VFT curve. Pascual observed that shorter glasses have lower viscosity values, which was attributed to the difficulty of accurate temperature measurements when viscosity changes rapidly with temperature, especially in the sintering range. [8]

Similar viscosity results to Scholze are observed for softening and half ball, but viscosities an order of magnitude lower for where 'first shrinkage' occurs. [8, 11] This discrepancy was attributed to the difference in particle size, pressing pressure, and heating rate. Scholze used glass powder of < 75 μm whereas Pascual et al. used powder with a d_{50}=12 μm, which may have delayed the onset of shrinkage. It is important to note that the first and maximum shrinkage points have the most uncertainty since the shrinkage is a function of packing, i.e., the particle size and pressure applied, as well as the skill of the

observer in establishing these points.[8] These irregularities are potentially avoided by using a standard packing pressure, a single particle size distribution, and a software that can more accurately determine area variance based on pixels.

Pascual et al. [8] conclude that HSM offers a quick simple method to confidently determine viscosity temperature curves for a wide range of glasses with acceptable error. However, several studies suggest that the temperatures that correspond to the characteristic viscosity points, especially for shrinkage, strongly depend on experimental conditions such as particle size and initial density. [8, 68] The preparation method of hand compaction of powders, as suggested by the HSM manual, is not sufficient in producing sample compacts of similar initial densities. Therefore, the results between separate experiments are not necessarily comparable.

F.   Heat Transfer

Thermal conductivity may be negligibly different for the glasses analyzed in the current work of similar preparation and composition. Additionally, the small sample size used for these experiments should limit thermal gradient concerns due to thermal conductivity. In other words, the temperature of the compact surface should not greatly differ from the bulk. However, if a temperature difference exists, it would be expected that the bulk temperature would lag behind the surface temperature.

Fourier's law defines thermal conductivity, K, as the amount of heat transmitted per unit cross-sectional area per unit time when a thermal gradient exists.[58] The flow of heat, under equilibrium conditions, can be represented by

$$Q = KA \left(\frac{dT}{dx} \right) \tag{20}$$

where Q is the heat current, or flux per unit time, A is the cross-sectional area, T is the temperature, and x is the linear direction of heat flow. Thermal conductivity of a glass occurs via phonon transport and is approximately 1 W/mK in the solid state. [58]The change in temperature with respect to position is represented by dT/dx. When there is no internal heat generation, the principle of energy conservation yields

$$\frac{dT}{dt} = \frac{d\left[\frac{\kappa dT}{dx} \right]}{dx} = \frac{\kappa \, d^2 T}{dx^2} \tag{21}$$

for transient flow. Thermal diffusivity, κ, is equal to thermal conductivity divided by density times specific heat capacity at a constant pressure such that

$$\kappa = \frac{K}{\rho C_P} \tag{22}$$

Approximate values of K and C_p are taken to be 1.0 W/mK and 850 J/kgK, respectively, for a borosilicate glass, from Yang et al.[69]. Assuming a density of 2230 kg/m^3, Yang et al.[69] calculates a thermal diffusivity of approximately 6.5 x10^{-7} m^2/s. Laubitz[70] proposed that the effective thermal conductivity *reduced* by 0.3-0.4 when in powder form.

EXPERIMENTAL PROCEDURES

A. Densification Investigation

1. Material Preparation

Glass compositions commonly designed for hermetic seal applications were obtained from Community Glass, Inc. (Elmira, NY). Glasses were batched, melted, and quenched before milling to <80 mesh (100% < 177μm). The silicate powders were mixed in water, but the borosilicate glass was mixed in isopropanol. Polyethylene glycol (Carbowax 20M PEG) was added as an organic binder. The slurries were then spray dried and the granules were sieved to obtain a narrow distribution between 74-250 μm in diameter for good flowability. The fine and coarse scalped ends were retained for the experiments evaluating the role of particle size on sintering behavior. The granulated powder was then pressed in a mechanical tablet press (Stokes Press Community Glass, Inc., Elmira, NY) into compacts 2.86 mm in diameter and approximately 2 mm in height. Small sample sizes limited the thermal gradient within the compact.

Constant initial density is critical for the comparison of various heating rates, and thus was kept constant for comparison. Different compact heights were produced by adjusting the upper plunger stroke distance, depending on the pressing pressure. This compact preparation produced geometrically similar samples and strong green bodies. The white and borosilicate glasses were pressed at relatively similar stoke lengths, while the blue glass appears to be pressed to a larger stroke distance, producing a compact of slightly greater pressed density. Since samples were pressed in a mechanical press, the exact pressure and stroke distance is unknown. However, because the initial relative densities were equal within a composition set, sintering behavior is comparable over various heating rates. A supplementary experiment evaluated the sintering behavior of three variations of initial density for a silicate glass, comparing compacts with a fixed fill and varying stroke distances.

Additional loose powder was retrieved for density measurements. Skeletal densities of the powders were measured using a pyncometry method (Accupyc II 1340, Micromeritics, Norcross, GA). Initial relative densities, based on the skeletal density, are

41

listed in Table I. Bulk densities were measured geometrically and assume zero porosity, but for the means of ensuring similar initial conditions, this assumption is acceptable. Masses were measured, after binder removal, in groups of ten compacts to improve the measurement precision.

Table I. Skeletal density, initial height, mass and relative density of the investigated glasses. Diameter was found to be 2.86 ± 0.008 mm for all cylindrical compacts.

Glass	Density (g/cm^3)	Height (mm)	Mass (mg)	Relative Density %
White	2.72	2.01 ± 0.02	24.7	70.4 ± 0.10
Blue	2.65	1.79 ± 0.01	22.8	74.2 ± 0.55
Borosilicate	2.18	2.06 ± 0.01	20.4	70.0 ± 0.08

2. Property Characterization

Table II lists glass transition temperatures and the published chemistries of the investigated glasses in mole %.[71-72] T_g was measured via vertical dilatometry of the sintered and annealed glass compositions using heating and cooling rates of 3 K/min. 'Blue glass' contains a small amount of cobalt, which results in the emission of blue. 'White glass' does not emit any color and is deemed a 'transparent' glass. A third glass containing approximately 22 mol% B_2O_3, referred to as 'borosilicate,' was also studied.

Table II. T_g and published chemistries of investigated glasses in mole %.[71-72]

Glass	T_g (°C)	SiO$_2$	B$_2$O$_3$	Al$_2$O$_3$	Na$_2$O	K$_2$O	Li$_2$O	BaO	CoO	P$_2$O$_5$
White	412	70.09	-	3.36	11.05	5.82	3.44	6.25	-	-
Blue	468	66.49	-	-	-	-	20.06	12.38	0.14	0.94
Borosilicate	480	60.55	21.78	1.24	2.0	1.31	4.14	-	-	-

3. Hot-stage Microscopy

Glasses were analyzed using a hot-stage microscope (HSM, Misura ODHT, Expert System Solutions version 3.32, 32-bit system, Modena, Italy). Powder compacts were heated in air in the HSM on an alumina substrate. Heating rates of 1, 3, 10, 30, and 60 K/min were executed. A dwell at 300 °C was maintained for 30 minutes for heating rates >3 K/min to guarantee complete binder burnout. Data acquisition intervals were time-based, ranging from one minute to one second, depending on the heating rate.

In a separate study, blue glass powder was separated into three different cuts, as in different scalped granule sizes, and the effect on sintering temperature was examined. Powder was sieved to obtain fine granules (<74μm), coarse granules (>250μm) and a distribution of scalped granules between 74 and 250 μm. All three granule selections were also pressed to three different densities; low, medium, and high pressed density. These variables were evaluated using a heating rate of 10 K/min.

i. Data Analysis

The peak sintering temperature, $T_{PS,}$ was calculated using a data smoothing technique in a spreadsheet (Microsoft Excel 2016 version 16.0.14026.20304 32-bit, Redmond, WA) of the area variance data as a function of temperature, defined here as a running slope. This approach constitutes a direct derivative of the raw dataset. The slope is calculated using an odd number of data points about a center point to avoid curve shift. The derivative of area variance with respect to temperature is labeled $d(AV_x)/dT$ with "x" denoting the number of data points incorporated into the derivative. An example of the data smoothing technique, as presented in Table III, calculates the slope of 7 data points. It should be noted that area variation is in units mm^2 and a negative area variation corresponds to expansion. The role of the number of data points incorporated into the running slope function is demonstrated in Figure 21. T_{PS} is denoted with an X in Figure 21. When the variability observed by the HSM is smoothed to form a coherent curve rather than a set of independent points, the peak sintering temperature is clearly identified. Initial shrinkage temperatures are chosen as point in the $d(AV_x)/dT$ curve before the sintering hump, as seen by circled datapoints in Figure 21. Similarly, the maximum shrinkage, or the temperature at which sintering is completed, denoted with a square, is chosen as the final point in the sintering hump after T_{PS}, indicating a halt in shrinkage as densification terminates but before bloating (the expansion of trapped gas remaining from packed bed porosity) is observed. Initial and maximum shrinkage temperatures are weakly dependent on the number of cycles. Initial shrinkage temperature decreases with increasing cycles in the slope calculation, while the maximum shrinkage temperature increases. T_{PS} and the initial and maximum shrinkage temperatures are not identified for the 3-cycle data plot.

Table III. An example of the data smoothing technique used in the current study, using a 7-cyle running slope calculation. (White glass, 10 K/min)

Temp. (°C)	Area Variation	Running Slope $d(AV_7)/dT$
550	7.31×10^{-2}	3.02×10^{-3}
551	7.51×10^{-2}	3.17×10^{-3}
552	7.85×10^{-2}	3.30×10^{-3}
553	8.10×10^{-2}	3.41×10^{-3}
553	8.39×10^{-2}	3.39×10^{-3}
554	8.61×10^{-2}	3.28×10^{-3}
555	8.97×10^{-2}	2.84×10^{-3}
556	9.15×10^{-2}	2.90×10^{-3}
557	9.55×10^{-2}	3.34×10^{-3}
558	9.58×10^{-2}	3.51×10^{-3}
558	10.0×10^{-1}	3.63×10^{-3}
559	10.4×10^{-1}	3.53×10^{-3}
560	10.6×10^{-1}	3.23×10^{-3}
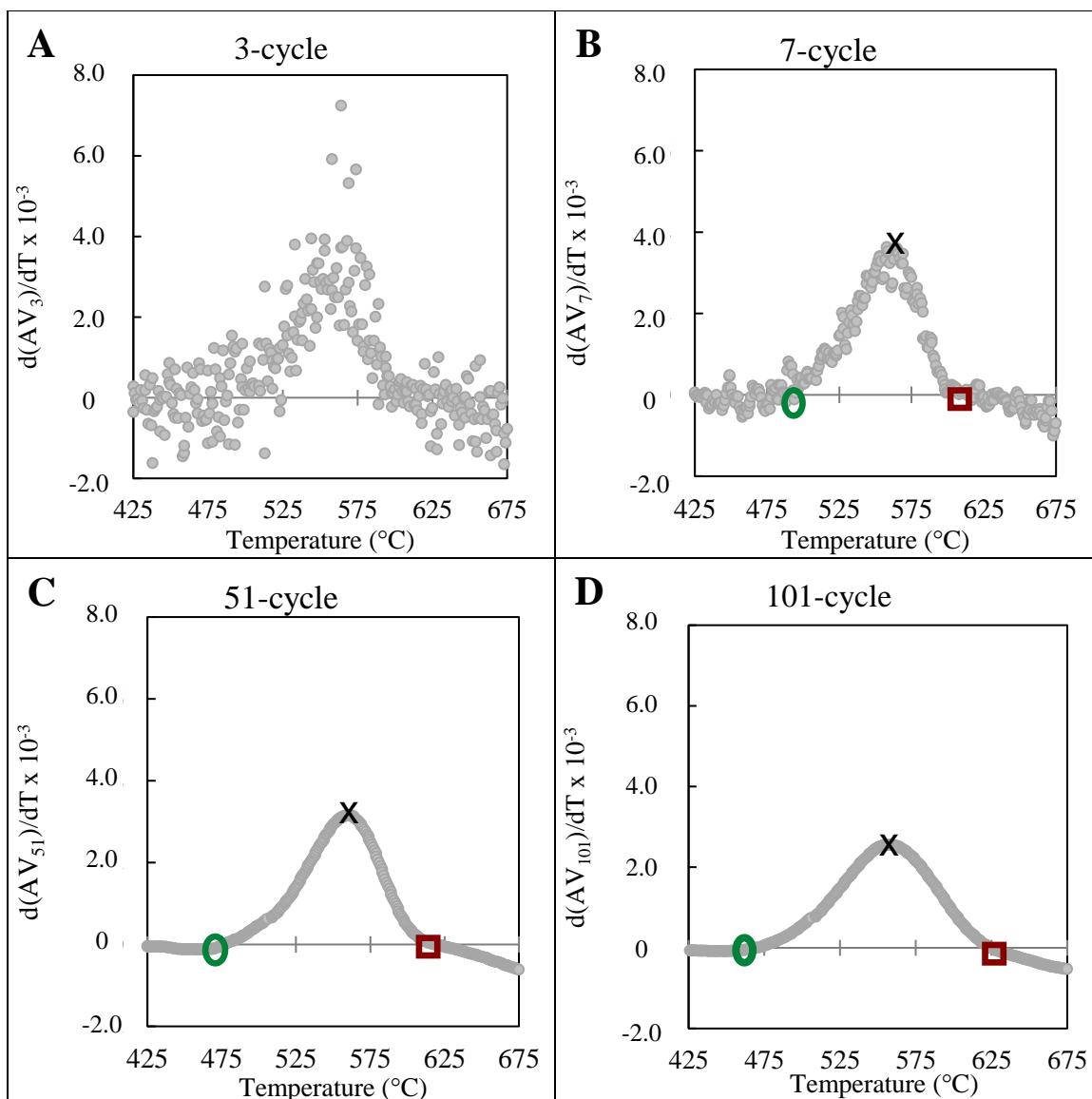
Figure 21. Example of data smoothing technique using a running slope of 3, 7, 51, and 101 data points. Scatter in the data decreases with increasing running slope cycles. However, the more subtle slope details may be lost with greater cycles. (White glass 10 K/min)

When the number of datapoints included in the running slope curve is increased, however, the variations between the captured images, or counted pixels, decreases and the clarity of the peaks improves. While increasing the data range included in the slope may result in the smoothing of more subtle changes in the area variance as a function of temperature, the precision of T_{PS} may improve, as evidenced by the smaller deviations between experimental runs demonstrated in Figure 22. Figure 22 depicts average T_{PS} as a function of slope cycles for three runs of the same test conditions and compositions for heating rates 1, 3, 10, and 30, demonstrating the repeatability of the HSM. The standard

deviation is a result of the multiple experiments run with the same conditions. 60 K/min is also included in Figure 22 but without standard deviation error bars (as this experiment was executed once). Increasing the data used in this calculation does not weaken the integrity of the peak sintering temperature, and it allows variance within the dataset to be measured. T_{PS} exhibits less variation when the running slope includes at least 21 data points in the calculation, as indicated in Figure 22. In this work, T_{PS} is designated as the average of the maximums in the $d(AV_{51})/dT$ curves. The standard deviations within the plot demonstrate the repeatability of this analysis technique. In order to obtain a standard deviation of this type of analysis, the peak sintering temperatures determined from $d(AV_{21})/dT$ to $d(AV_{101})/dT$ are averaged and standard deviation is calculated.
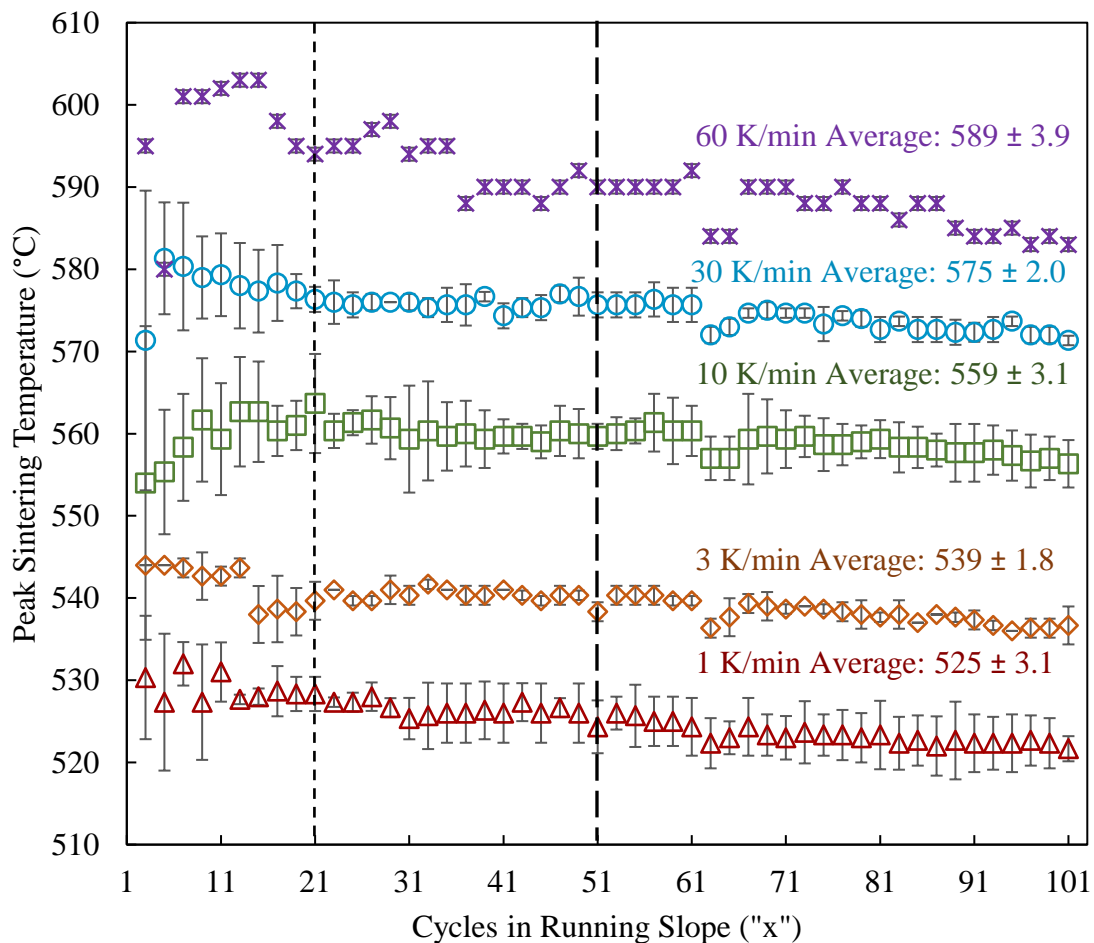
Figure 22. Peak sintering temperature as determined by the number of data points in used in the running slope calculation. The average peak temperature remains fairly consistent above 21-cycles. Three experimental runs with heating rates 1-30 K/min were completed, 60 K/min experiment was completed once.

Figure 23 shows area variance (left y-axis) as a function of temperature. The derivative of the raw dataset, corresponding to the right y-axis, is labeled $d(AV_{51})/dT$ to describe the derivative of area variance with respect to temperature using 51 data points in the slope calculation. This curve demonstrates the change in slope of the area variance curve, in addition to smoothing out the variability observed by the HSM. The 'sintering range' captures the temperature range from initial to maximum shrinkage, determined from the derivative of area variance. T_{PS} corresponds to the maximum in the $d(AV_{51})/dT$ curve and the inflection point of the area variance curve, i.e., just before sintering slows as pores close and the driving force for sintering transitions from surface area reduction to the surface tension driven elimination of pores.[3-4] However, the sintering behavior is proposed to follow the Frenkel model until nearly 655°C, when the slope of the derivative of the area variation curve deviates from a nearly symmetrical hump. This point is potentially the start of where the Mackenzie-Shuttleworth (MS) model can describe the sintering behavior; all pores are closed and densification is a direct result of pore shrinkage. (Although, it is debatable if spherical pores can be eliminated solely by diffusion of gas.) Alternatively, the a combination of Frenkel and Mackenzie-Shuttleworth behavior as described by the Clusters model[51] for polydispersed particles may represent shrinkage behavior from the T_{PS} to the proposed temperature where the system reaches closed porosity.
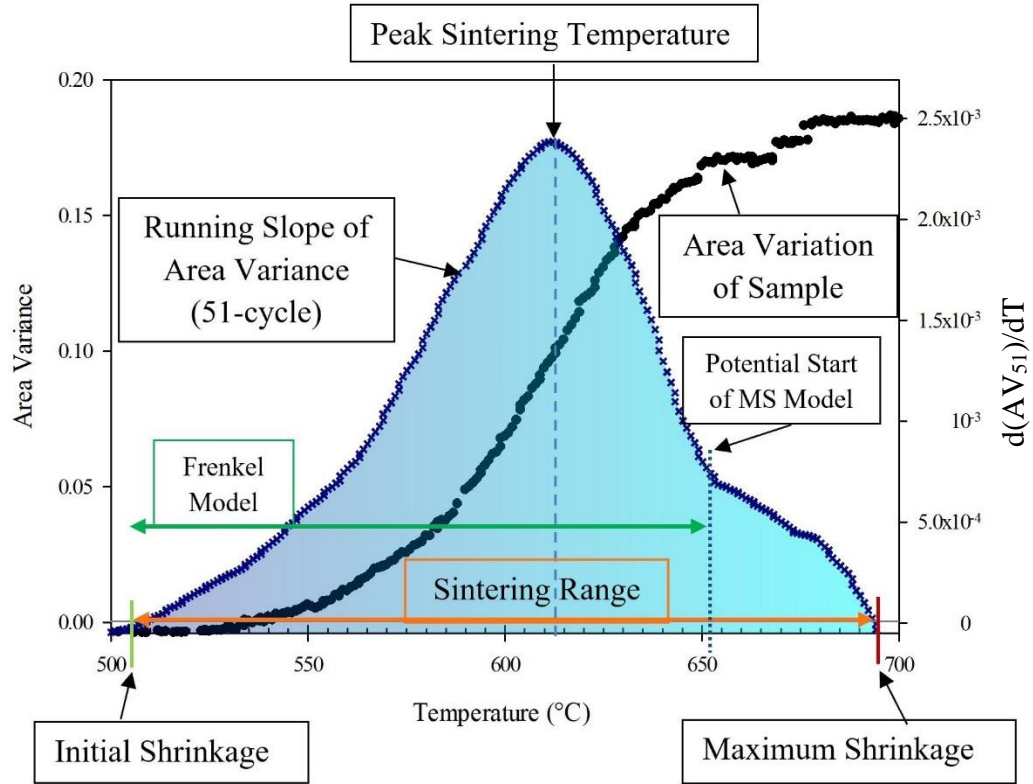
Figure 23. An example of the area variance as a function of temperature plotted with $d(AV_{51})/dT$. T_{PS} corresponds to an inflection point of area variance curve. The Frenkel model potentially describes the sintering behavior until nearly 655 °C. Further sintering behavior may follow the Mackenzie-Shuttleworth (MS) model. (Blue glass 10 K/min)

It is proposed that sintering temperature is a function of accumulated thermal energy, or 'heat work', within the sample. Heat work considers the amount of time spent at temperature, and thus can be crucial to determining the effect of heating rate on sintering temperature. Thus, the area under the curve, considered here as the 'heat work,' is calculated from the time and temperature at which the expected glass transition temperature is reached to the time and temperature at which peak sintering is reached. It is also proposed that heat work is a function of logarithmic time, implying that sintering temperature is a function of logarithmic heating rate. To evaluate this proposal the areas under the curve were calculated and compared using both time on a normal scale rather than time on a logarithmic scale. Figure 24 illustrates this area under the curve being investigated.
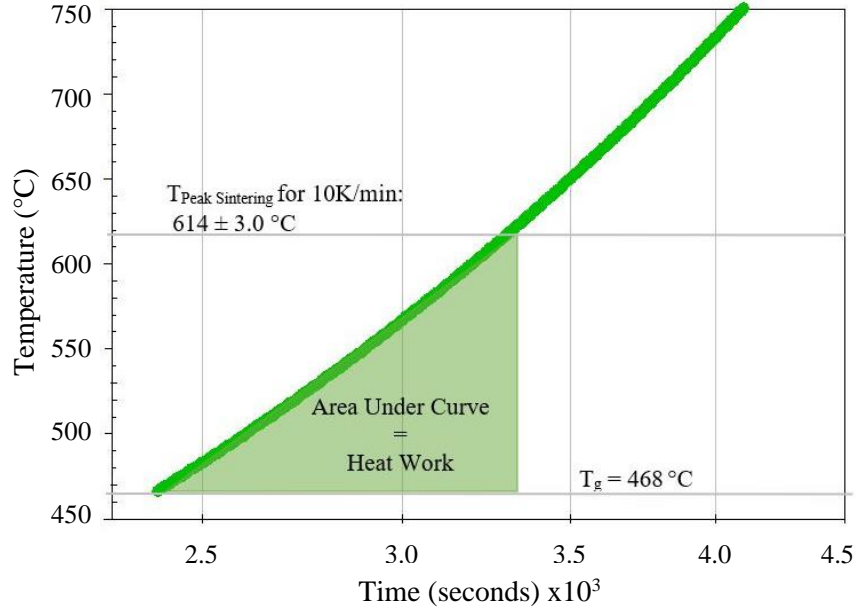
Figure 24. Example of the area under the curve of the temperature as a function of time on a logarithmic scale plot from T_g to T_{PS} for blue glass heated at 10 K/min.

The area under the curve is calculated, assuming a triangle and using the equation

$$\tfrac{1}{2}\,(T_{\text{peak sintering}} - T_g) * (t_{\text{peaksintering}} - t_{Tg}) \tag{23}$$

And

$$\tfrac{1}{2}\,(T_{\text{peak sintering}} - T_g) * \log(t_{\text{peaksintering}} - t_{Tg}) \tag{24}$$

T_g is chosen as the lower limit because viscous flow is expected to be insignificant below this temperature and thus negligible densification occurs below T_g. It should be noted that faster heating rates will yield higher glass transition temperatures.[61, 65] However, this work assumes no change in glass transition temperature with heating rate and appears to have no significant influence on the calculated heat work.

RESULTS AND DISCUSSION

A. Influence of Heating Rate

Faster heating rates appear to delay the onset of shrinkage and thus indicate greater sintering temperatures, as reported in Table IV. White and borosilicate glass compacts were pressed to similar initial densities, while blue glass was pressed with slightly greater initial densities. However, all samples within the same composition set were pressed with equivalent pressures and thus have similar initial densities, allowing the comparison of sintering behavior comparison between various experiments of the same composition. Initial shrinkage temperature is the temperature at which shrinkage begins. Peak sintering temperature identifies the fastest shrinkage rate observed. Maximum shrinkage temperature is defined as when shrinkage ceases, i.e., the end of the sintering and the start of bloating.

Table IV. Average peak sintering temperatures, initial and maximum shrinkage temperatures of white, blue and borosilicate glass at various heating rates.

	Sintering (and Shrinkage) Temperatures (°C)								
	white glass			blue glass			borosilicate glass		
Rate K/min	Initial	Peak	Max	Initial	Peak	Max	Initial	Peak	Max
1	442±1.1	525±3.1	582±3.5	484±1.7	576±1.3	635±0.3	562±13	696±2.7	758±2.7
3	458±5.3	539±1.5	602±2.3	484±17	589±2.4	659±1.3	569±13	707±2.9	774±1.8
10	476±3.1	559±3.1	620±2.1	507±1.7	614±3.0	695±2.5	547±41	722±2.8	803±11
30	472±8.5	575±2.0	651±1.0	509±20	636±3.4	721±7.1	599±11	738±3.6	805±1.2
60	490±18	589±3.9	648±4.3	536±6.4	649±3.5	722±6.2	581±10	743±2.8	822±1.0

Figure 25A shows the area variance as a function of temperature for white glass as the compacts are heated at various rates. Note that an increase in area variance (positive slope) reflects shrinkage while a negative slope indicates expansion. The slope of this curve decreases with increasing heating rate. Figure 25B shows $d(AV_{51})/dT$ as a function of temperature for various heating rates. The initial and maximum shrinkage temperatures shift to higher temperatures with increasing heating rate. The sintering peaks are not only shifted to higher temperatures, but also decrease in height and broaden in width, in agreement with the decreasing slopes at higher heating rates shown in Figure 25A. Similar results for blue glass and borosilicate glass are presented in Figures 26 and 27, respectively.
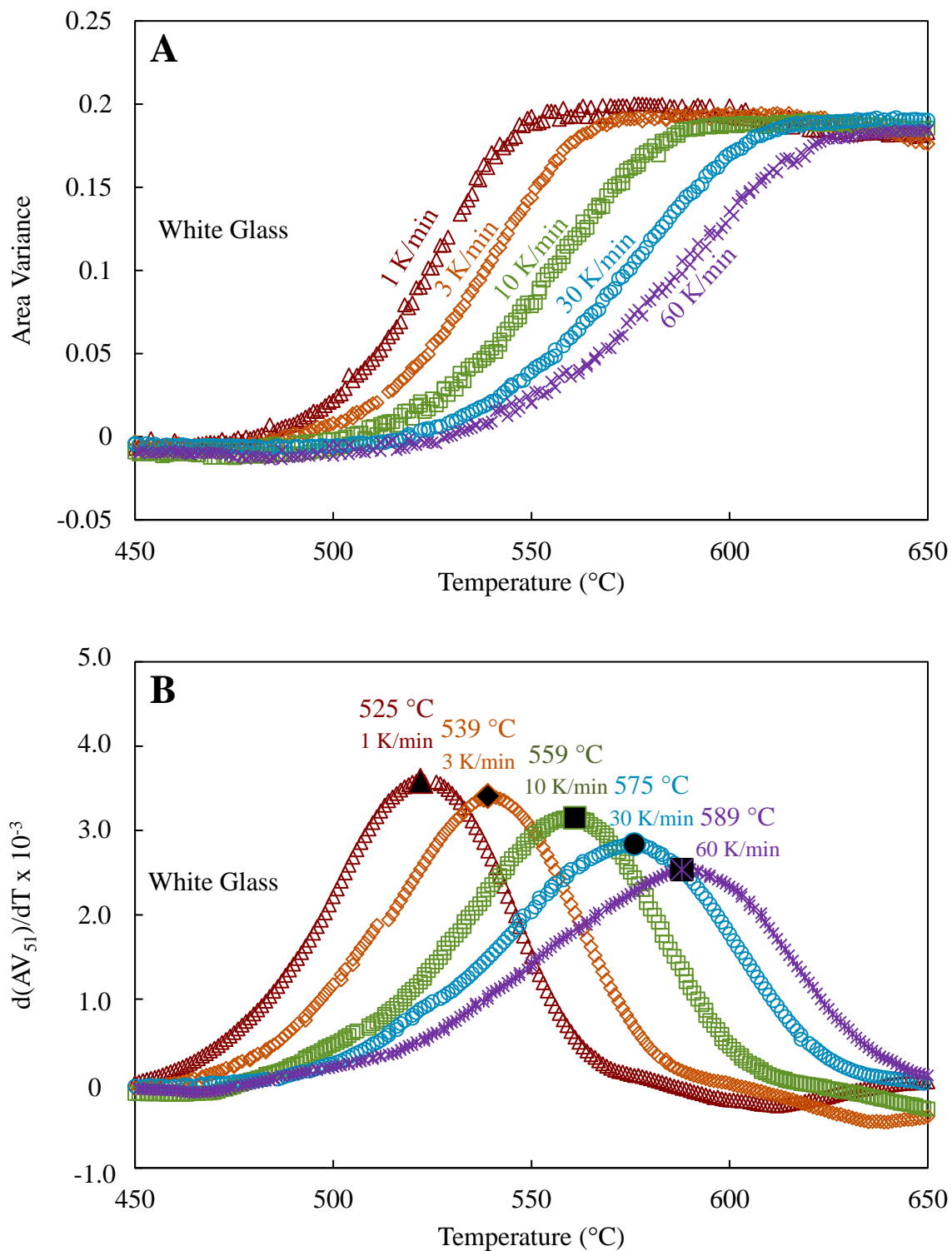
Figure 25. A) the area variance and B) $d(AV_{51})/dT$ as a function of temperature for white glass, indicating peak sintering temperature for each heating rate.
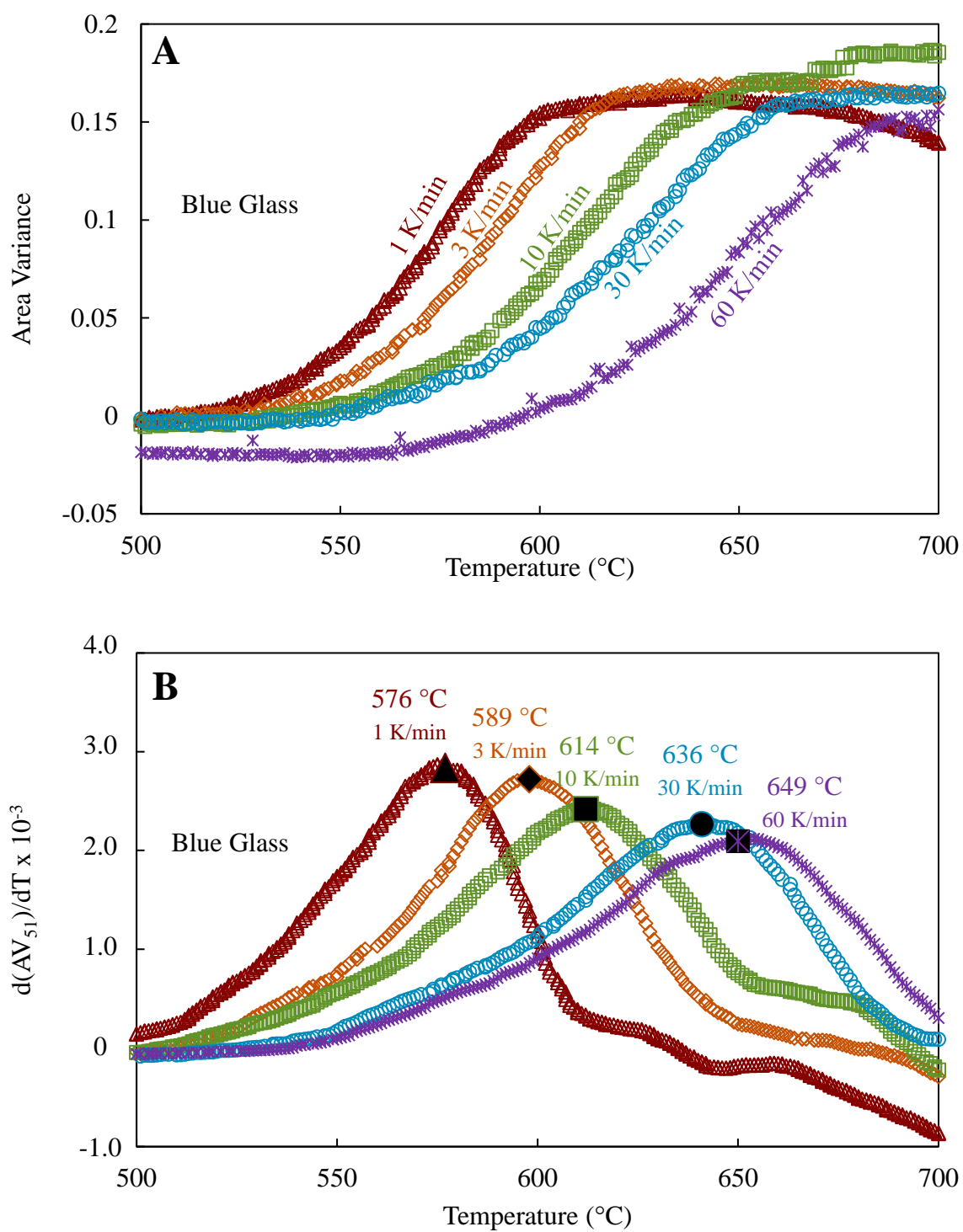
Figure 26. A) the area variance and B) d(AV$_{51}$)/dT as a function of temperature for blue glass, indicating peak sintering temperature for each heating rate.
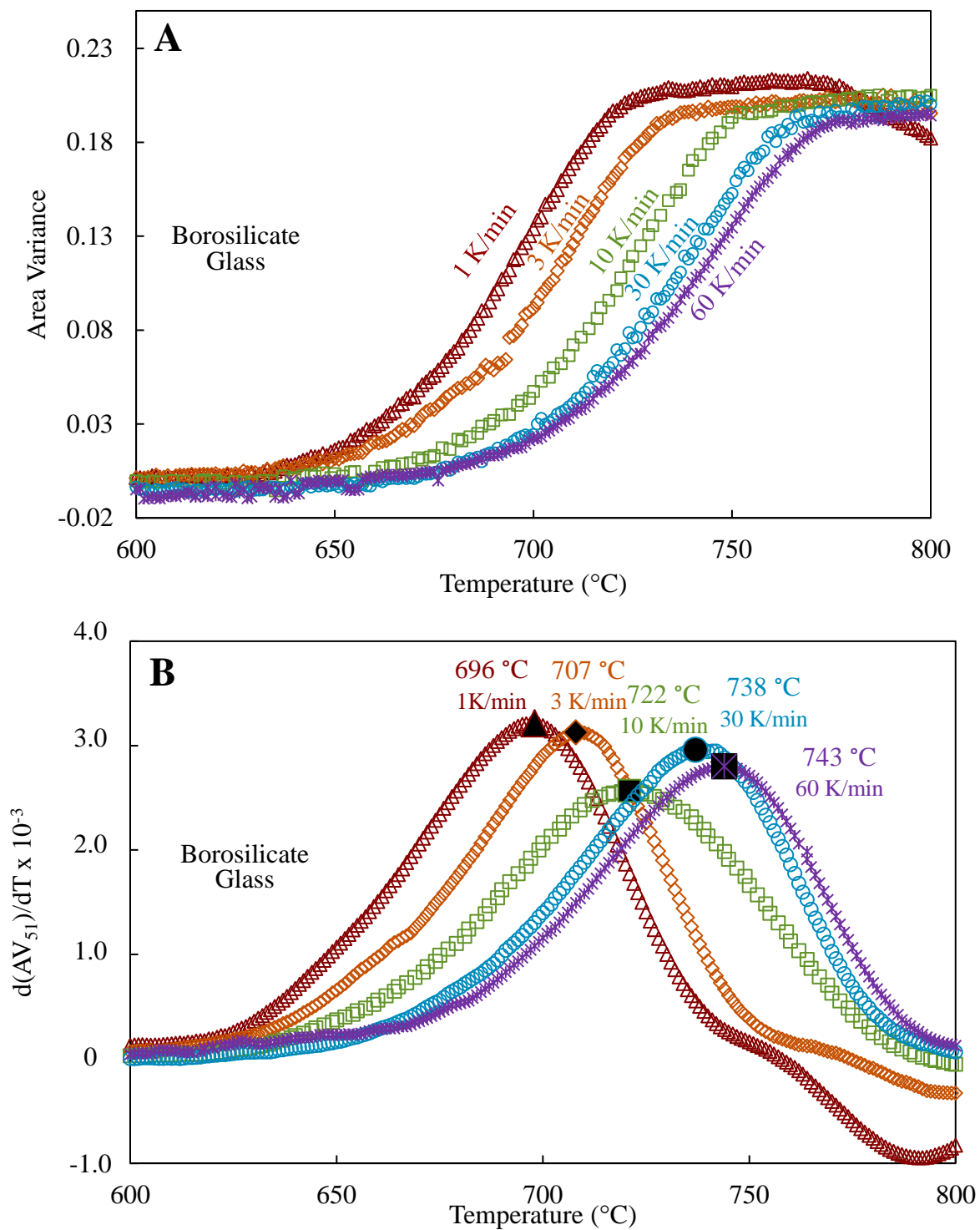
Figure 27. A) the area variance and B) $d(AV_{51})/dT$ as a function of temperature for borosilicate glass, indicating peak sintering temperature for each heating rate.

Figure 28A compares the three glasses when area variance is normalized by initial height and temperatures are normalized by T_g for a heating rate of 3 K/min. Normalized $d(AV_{51})/dT$ is plotted as a function of temperature in Figure 28B. The ratios of sintering temperature to glass transition temperature are similar for blue and white glass, (T_g:T_{PS} of 1:1.26 for blue and 1:1.31 for white) but the borosilicate glass has a significantly greater ratio of T_g:T_{PS} at 1:1.48. This data agrees with the viscosity-temperature relation, seen in Figure 2, where the temperature difference from a glass transition viscosity to a sintering viscosity is greater for a typical borosilicate glass compared to SLS glass.
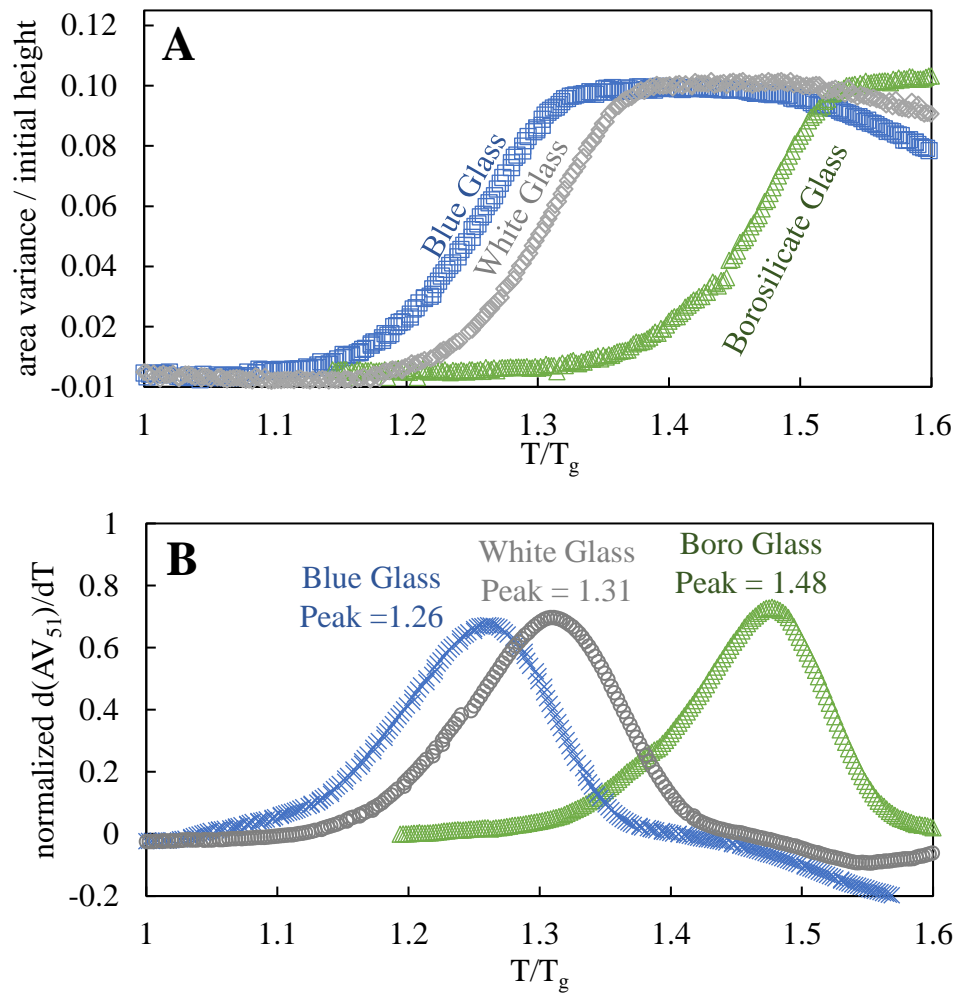
Figure 28. A) Area variance (normalized by the initial height of the sample) as a function of temperature normalized to the glass transition temperature for blue, white, and borosilicate glass heated at 3 K/min. B) the derivative of A with respect to temperature.

The ratio of T_g to T_{PS} increases with increasing heating rate, as seen in Figure 29. The peak sintering temperatures trends are plotted normalizing the sintering temperature

to the glass transition temperature. The sintering temperatures of borosilicate glass appear to have a weaker dependence on heating rate than blue and white glass.
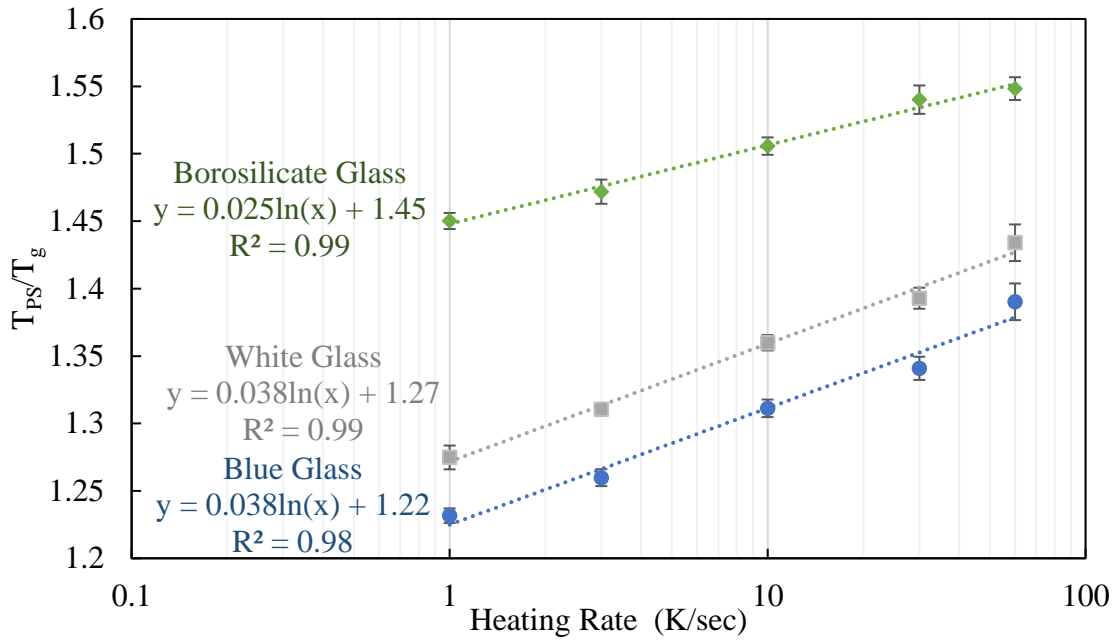
Figure 29. T_{PS} normalized by T_g plotted as a function of heating rate.

Initial and maximum shrinkage temperatures and peak sintering temperatures as a function of heating rate for white, blue, and borosilicate glasses are presented in Figure 30. Though these plots appear similar, when the slopes of the best fit lines for initial shrinkage, T_{PS} and maximum shrinkage temperatures are plotted as a function of y-intercept (normalized to T_g), it is clear that borosilicate glass behaves differently than the blue and white glass, as seen in Figure 31.
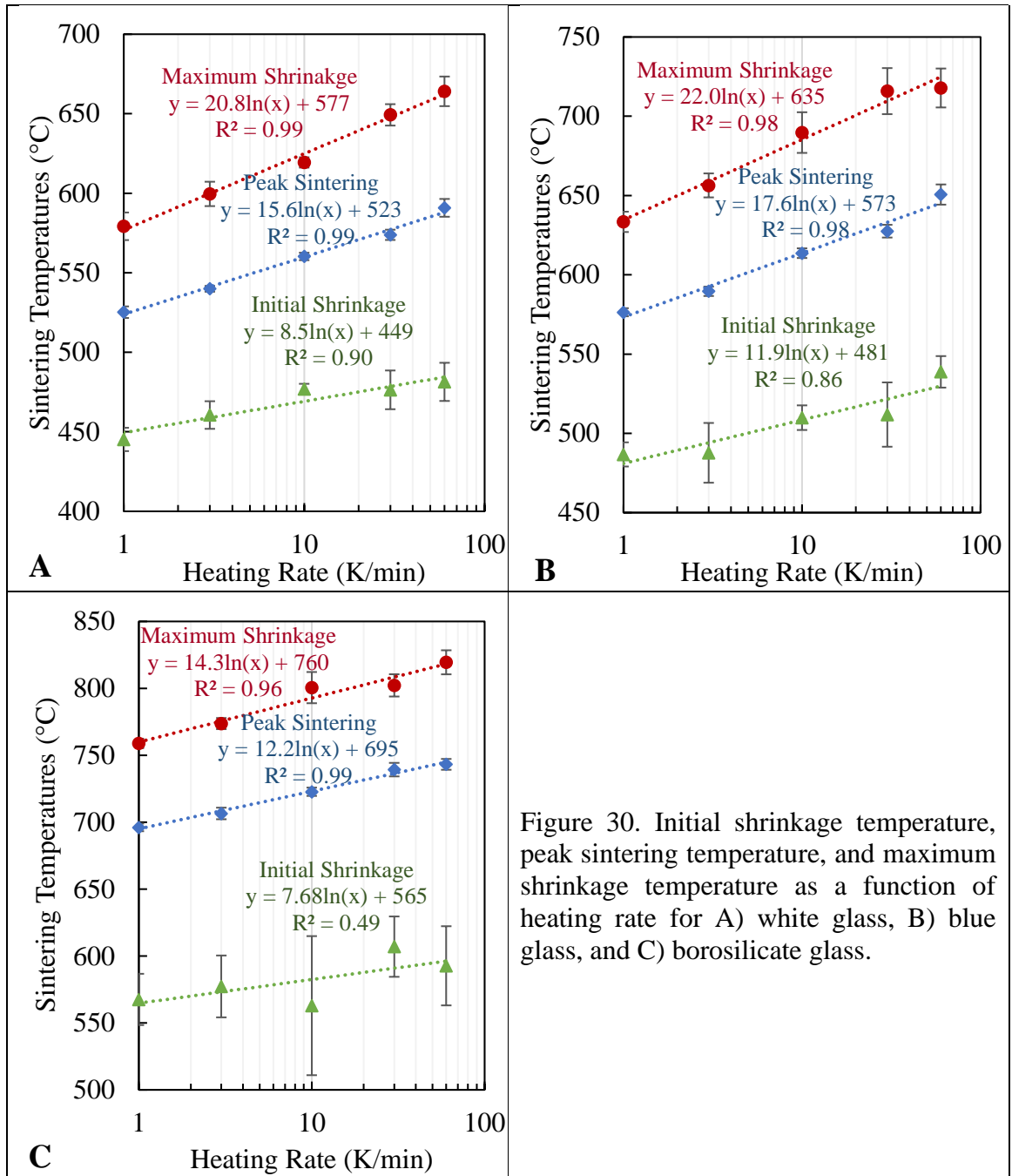
Figure 30. Initial shrinkage temperature, peak sintering temperature, and maximum shrinkage temperature as a function of heating rate for A) white glass, B) blue glass, and C) borosilicate glass.
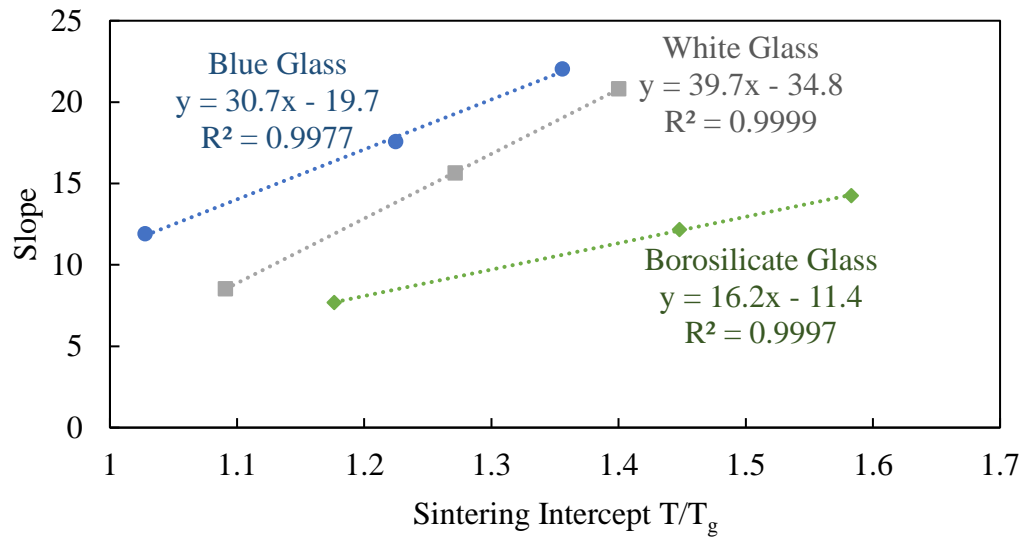
Figure 31. The slopes of the best fit lines of Figure 30 plotted against the y-intercept normalized by T_g of each glass.

B. Heat Work

While the recorded sintering temperature is indicative of the average kinetic energy of the particles in the air surrounding the thermocouple, it does not represent the average temperature of the entire sample. For instance, at 1 K/min, it is likely that the sample can reach an equilibrium temperature throughout the compact, equal to that of the surrounding air, whereas at 60 K/min, the average temperature of the sample will likely lag behind the temperature recorded by the thermocouple. The rate of temperature change of the sample is dependent on the thermal conductivity of the material and the heating rate. Thus, the amount of thermal energy accumulated over a period of time may be more appropriate when comparing samples with different heating rates. The combined effect of temperature and time is termed 'heat work.' [73] Pyrometric cones were invented to assess the heat work in the firing of traditional ceramic bodies such as porcelain and stoneware. Heat work was measured in pyrometric cones by the viscous deformation. [73-74] Pyrometric cones demonstrate that soaking a furnace at a lower temperature generated a densification result similar to that observed for a shorter time at higher temperature. The amount of heat work, or thermal energy, required for viscous sintering to occur should be similar for all heating rates. Therefore, the area under the curve should remain constant.

Heat work may be calculated by determining the area under the curve from the transition temperature, T_g, to the observed sintering temperature, T_{PS}, with units degree · time (K·s). This is illustrated by the shaded area under the curve in Figure 32. When time is plotted on a normal scale the areas of the triangles decrease as heating rate increases. The products of the approximate areas under the curves are listed in Table V, calculated using Equation 23. The relation of decreasing area with increasing heating rate is plotted in Figure 33.
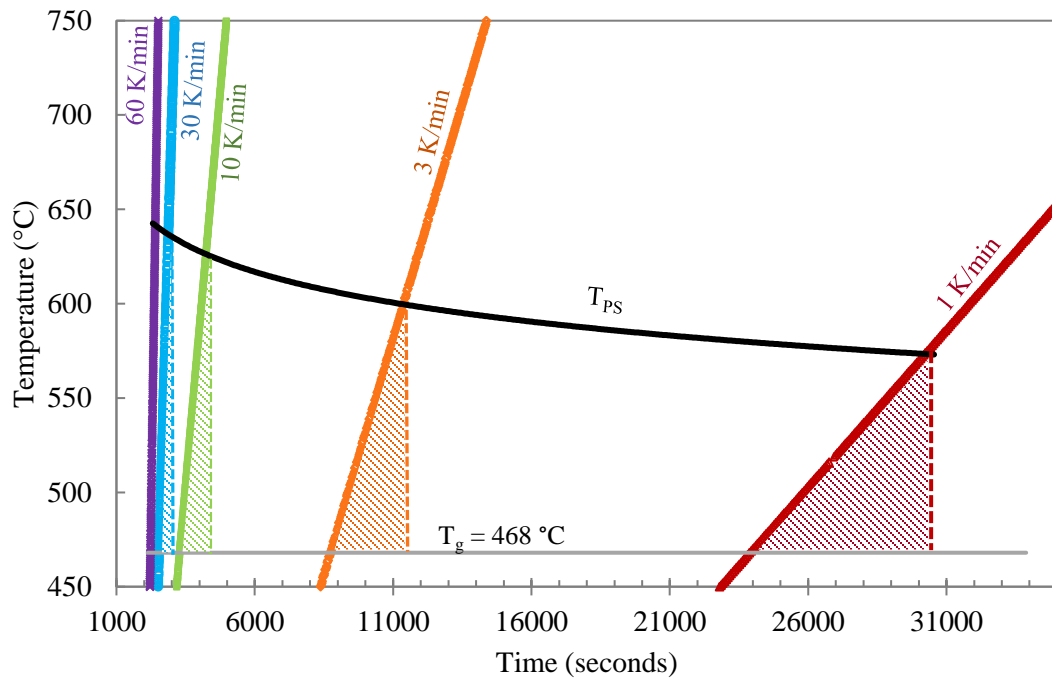
Figure 32. Temperature as a function of time illustrating the heat work required for various heating rates calculated by the area under the curve from T_g to T_{PS}.

Table V. Area under the temperature-time curve from peak sintering temperatures to the expected T_g with units K·sec, calculated for time plotted on a normal scale.

Heating Rate		White Glass	Blue Glass	Borosilicate Glass
		Area Under Curve	Area Under Curve	Area Under Curve
K/min	K/sec	From T_{PS}– 412°C x 10^4	From T_{PS}– 468°C x 10^4	From T_{PS} – 480°C x 10^4
1	0.02	37.0	37.6	140
3	0.05	16.4	17.1	51.5
10	0.17	6.44	6.50	17.5
30	0.5	2.90	2.90	6.68
60	1	1.70	1.58	3.42
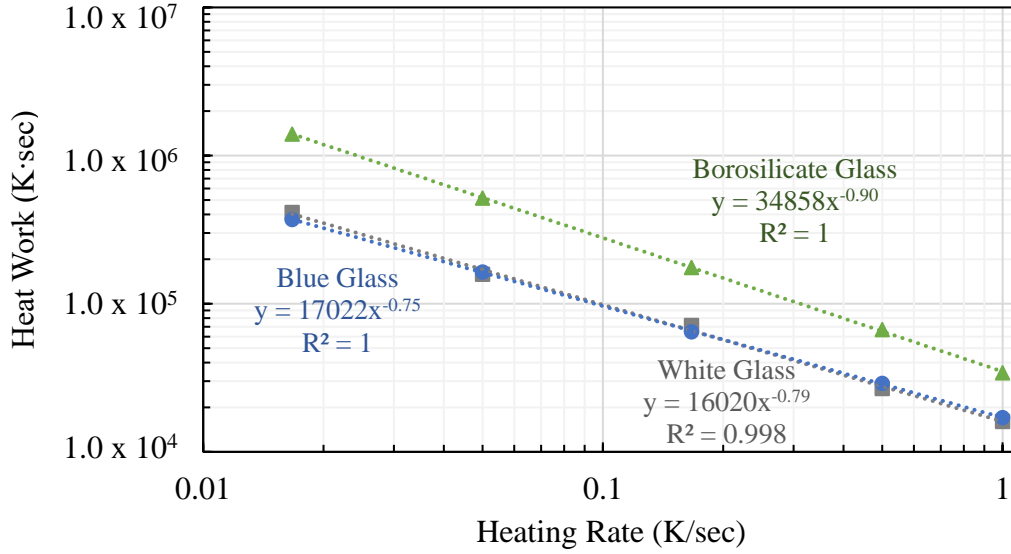
Figure 33. Relation of the approximate area under the curve (calculated with normal time) with heating rate (K/sec) for the three investigated glasses with both axes plotted on a log scale.

Lerdprom[75] found a log-dwell time dependence for the silica level in a porcelain glass as well as the coarsening behavior of mullite crystallites, in the sintering of a porcelain body. The increase in the silica level was due to quartz dissolution into the porcelain glass phase that progressed linearly with temperature but with the logarithm of soak time. He did not observe any measurable contribution of heating rate on densification temperature. However, it is proposed that in the absence of a soak at peak temperature, heating rate substitutes for soak time. Thus, it is proposed that heat work for non-isothermal conditions also follows a log-heating rate relationship.

When temperature is plotted against the logarithm of time (Figure 34), T_{PS} for each heating rate scales linearly with log-time. Heat work, calculated assuming the area of a triangle (Eq. 24) as discussed above, exhibits a relatively constant area when calculated using logarithmic time, as seen in Table VI. Approximate heat work, calculated assuming the area of a triangle, as a function of heating rate is plotted in Figure 35 for all three glasses. Heat work is relatively constant at 217 ± 10.4 K·log(sec) for white and blue glass, but decreases with increasing heating rate for borosilicate glass. This suggests that the heat work evaluated for logarithmic time is essentially constant for silicate glasses and that the temperatures at which viscous flow sintering occurs is a function of time on a logarithmic scale.

59
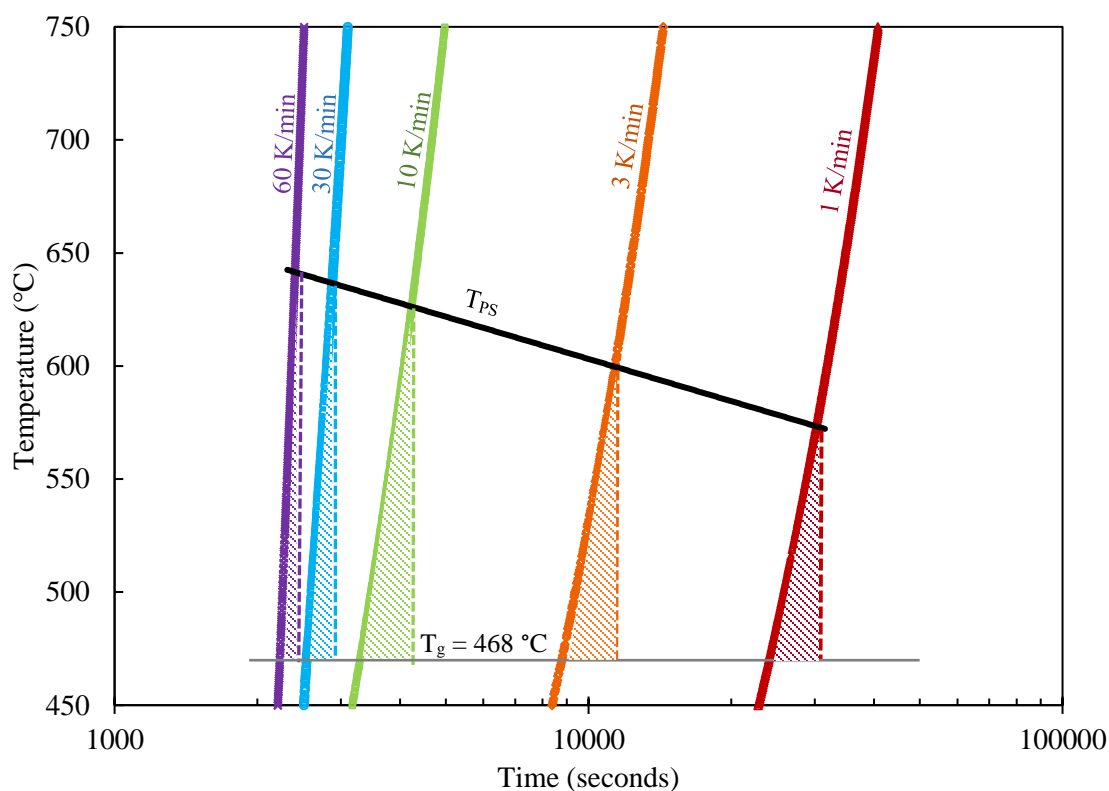
Figure 34. Temperature as a function of time on a logarithmic scale, illustrating the area under the curves calculated by the approximate area of a triangle from T_g to T_{PS}.

Table VI. Area under the temperature-time curve (heat work) from T_{PS} to the expected T_g calculated for logarithmic time (K·log(sec)).

Heating Rate		White Glass Area Under Curve	Blue Glass Area Under Curve	Borosilicate Glass Area Under Curve
K/min	K/sec	From T_{PS}-T_g (T_g= 412°C)	From T_{PS}-T_g (T_g= 468°C)	From T_{PS}-T_g (T_g= 480°C)
1	0.02	226	214	444
3	0.05	214	224	415
10	0.17	228	217	383
30	0.5	208	230	351
60	1	204	200	318
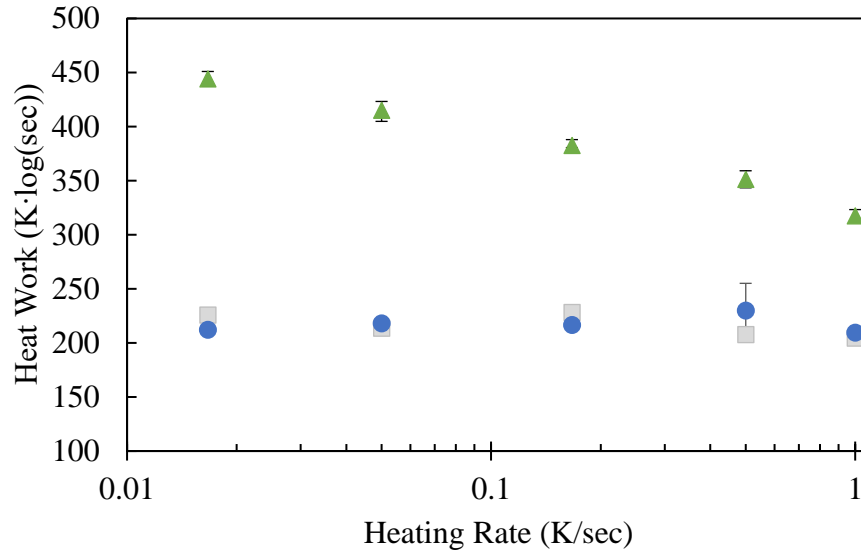
Figure 35. Approximate area under the curve for logarithmic time as a function of heating rate for borosilicate glass (green triangles), blue glass (blue circles) and white glass (gray squares).

It has been reported that values of T_g measured will depend on the heating rate of the dilatometric experiment, such that faster heating rates result in greater apparent T_g.[61, 65] Since T_g in this work was measured at 3 K/min, it follows that the area under the curve for 1 K/min is slightly less than 3 because it under estimates the height of the triangle. Similarly, the heights of the 30 and 60 K/min experiments, and therefore the calculated areas under the curves, are overestimated. However, the differences appear to be negligible.

i. Thermal Lag

The amount of time it takes for the temperature of the outside of the specimen to equal the temperature of the inside of the specimen depends on geometry and material properties, but according to Hsieh,[74] is constant and independent of heating rate. Thermal lag time is the difference between surface temperature and internal temperature divided by the heating rate. Following Fourier's heat conduction law, the time for temperature to move through a material is inversely proportional to the thermal diffusivity. The sample temperature is assumed to be uniform throughout the sample and equal to the furnace temperature, but if thermal lag time is constant then faster heating should result in higher *apparent* sintering temperatures.

However, a simple calculation refutes Hsieh's proposal. For example, if for every degree increase in temperature on the surface of the sample, it takes 0.333 seconds for the heat to reach the inside and the temperature to equilibrate. Assuming the heat transfers over a 1 mm distance, the heat transfer rate would be 0.333 mm/s. Thus, if the sample was at 25 °C and the furnace turned on and raised the temperature to 28°C, it would take about one second for the internal temperature to reach 28°C, *regardless of the furnace heating rate*. Figure 36 depicts the temperature difference from the surface to the bulk as temperature is increased for the conditions where it takes 0.333 and 0.1 seconds for the temperature of the center to reach that of the surface with heating rates of 10 and 60 K/min. The temperature difference between the surface and the center are compounded over time causing serious thermal lags at high heating rates. The slope of the line is equal to the time it takes for the heat to reach the center (sec) times the heating rate (K/sec).
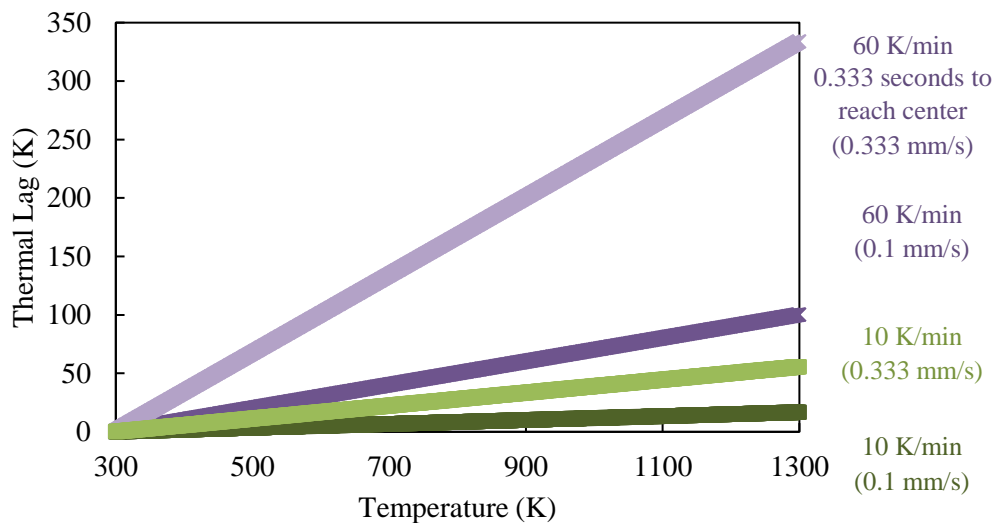
Figure 36. The thermal lag, or temperature difference between the surface and the center of the compact (assuming a 1 mm distance), for the conditions where it takes 0.333 and 0.1 seconds for heat to reach center of the compact, as temperature increases at constant heating rates 10 and 60 K/min (0.167 and 1 K/sec).

Various heat transfer rates are considered for the constant heating rate of 60 K/min in Figure 37. If it took 0.1 seconds for the heat to reach the center of the compact, after heating the sample 1000 degrees, the cumulative thermal lag would yield a temperature difference of 100 degrees between the surface and the center. Similarly, if the time for heat

to transfer from the surface to the center was 0.001 seconds, after heating 1000 degrees, the center of the sample would only lag 1 degree from the surface temperature.
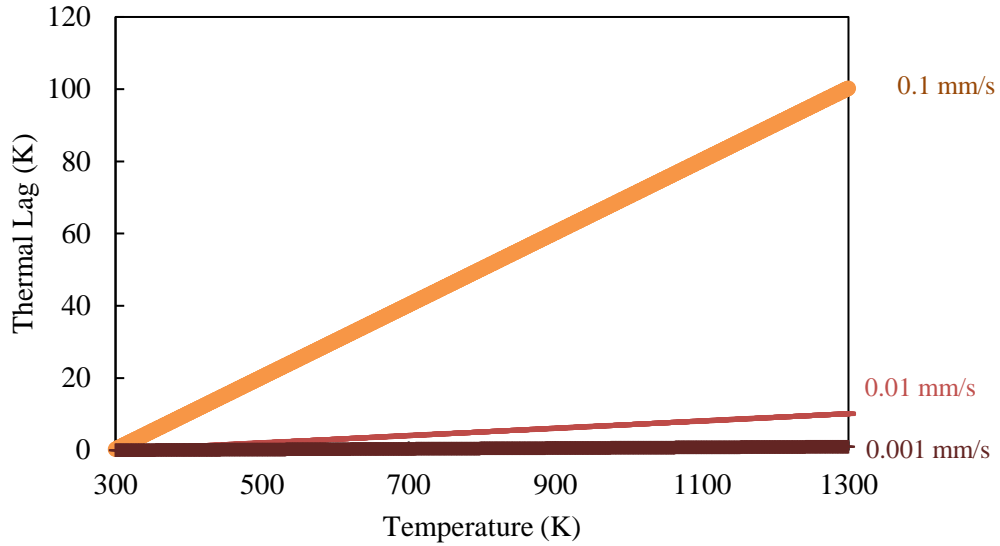
Figure 37. The thermal lag, or temperature difference between the surface and the center of the compact (assuming a 1 mm distance for heat to travel), for heat transfer conditions of 0.1, 0.01, and 0.001 mm/s for a constant heating rate of 60 K/min (1 K/sec).

C. Activation Energy

Following the activation energy analysis technique of Karamanov et al., plotting $\ln(v/T_x^2)$ versus $1000/RT_x$ the slope of the line corresponds to the activation energy for sintering.[33] Figure 38 is an example of this method, where T_x is the peak sintering temperature, as identified previously using the running slope method, for various heating rates (1, 3, 10, 30, 60 K/min) for the white, blue and borosilicate glass. Table VII lists the activation energies for initial, peak, and final sintering for the three glasses.
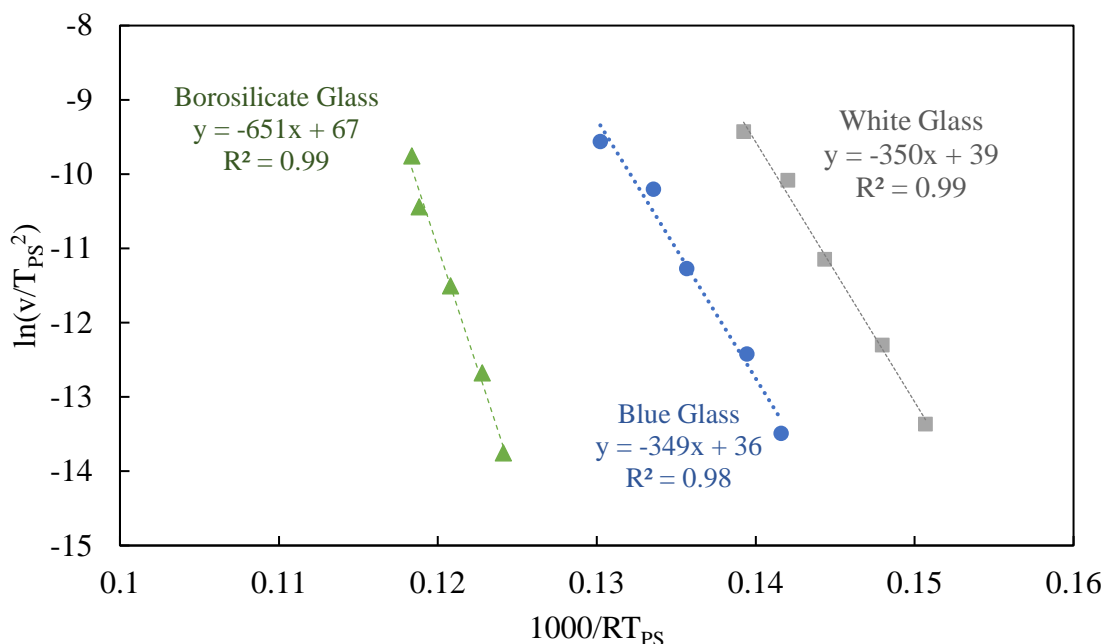
Figure 38. Activation energy calculated from the slope of $\ln(v/T_{PS}^2)$ as a function of $1000/RT_{PS}$ for various heating rates (1, 3, 10, 30 and 60 K/min) of borosilicate, blue and white glass.

Table VII. Activation Energies for Sintering (kJ/mol) Using Heating Rates 1, 3, 10, 30, and 60 K/min.

Sintering	White Glass	Blue Glass	Borosilicate Glass
Initial	459	359	376
Peak	350	349	651
Maximum	302	217	609

Activation energies for peak sintering temperatures for silicate glasses agree relatively well with published values for activation energy of sintering of silicate glasses.[32-33] Borosilicate glass has a nearly two times greater activation energy.

D. Influence of Pressed Density and Granule Size

Pressing samples at a constant pressure is a reproducible and more reliable method than the experimental specifications included in the HSM manual, which suggest hand pressing powders. In this study, a mechanical press is used to form powder compacts. Mechanical controls set punch stops to a particular displacement, not a particular pressure.[76] Although the pressing pressure is unknown, the die fill is fixed and the stroke of the top punch is changed to change the compaction level. The pressure resulting from displacement of the

moving punches compact the granulated powder into a pressed part. The fill is also unknown in this study, but is kept constant for each set of granules. Thus, if punch displacement increases, the fill is more compacted and the resulting pressed sample height decreases and density increases. The compaction ratio, CR, is the height of the fill (before pressing) divided by the height of the pressed compact.

With a fixed fill (fixed mass), if the stroke of the top punch used to press compacts increases, the height of the pressed pellet will decrease and thus increase the pressed density. However, stroke displacement was not constant between granule sets, e.g., low-density fine granules did not experience equivalent stroke displacements as low-density coarse granules. Nonetheless, the effect of relative pressed density on sintering temperature of each granule size distribution can still be analyzed separately since all granule sets have qualitative low- medium- and high- density compacts.

The average pressed height of each compact relative to the (qualitative) stroke length and granule size is listed in Table VIII. Ten compacts of each granule size were measured for height and diameter. Masses of the compacts after binder burnout but before sintering were measured by massing all ten compacts at once due to the small volume size and precision of the scale. Then the mass of ten samples was divided by ten to calculate the average mass of a single compact. Scalped refers to compacts with a granule size between 250μm and 74μm, coarse refers to compacts with granules >250μm, and fine refers to compacts with granules <74μm. Relative pressed densities (% of theoretical) are based on the geometrical bulk density of the pressed compact (mass recorded after debinding) divided by the skeletal density determined by He-Pyncometry. A heating rate of 10 K/min was used to determine the sintering temperature of various pressed densities.

Table VIII. Theoretical densities of powder compacts with various granule distributions. Diameter remains constant for all compacts at 2.87 ± 0.008 mm. Skeletal density (from He-Pyncometry) = 2.648 ± 0.0027 g/cm^3.

Blue Glass Granule Distribution	Stroke	Height (mm)	Mass[†] (mg)	Relative Density %
74 < d < 250μm (scalped)	short	2.53 ± 0.04	22.5	52.2 ± 0.74
	medium	2.00 ± 0.02	22.8	66.5 ± 0.79
	long	1.79 ± 0.01	22.8	74.2 ± 0.98
d < 74μm (fine)	short	2.64 ± 0.01	21.8	48.6 ± 0.21
	medium	2.09 ± 0.02	22.0	62.0 ± 0.79
	long	1.73 ± 0.01	22.0	74.6 ± 1.3
d > 250μm (coarse)	short	1.87 ± 0.01	21.4	67.3 ± 0.32
	medium	1.76 ± 0.01	21.3	70.8± 0.52
	long	1.67 ± 0.01	21.4	74.8 ± 1.1

Area variance as a function of temperature for various pressed densities for scalped granules is presented in Figure 39A. Figure 39B is the derivative of area variance versus temperature for scalped particles of various pressed densities. High (relative pressed) density samples exhibit the least shrinkage and low pressed density samples exhibit the greatest shrinkage (softer samples have more shrinkage). If particle rearrangement is required, it may be more difficult to facilitate when the sample has high initial density and large imposed stresses. Peak sintering temperature is also shifted to higher temperatures as pressed density decreases. Similar results are presented in Figure 40 for fine granules.

[†] Masses were measured by tens of compacts and divided by 10 to calculate the average mass of a single compact
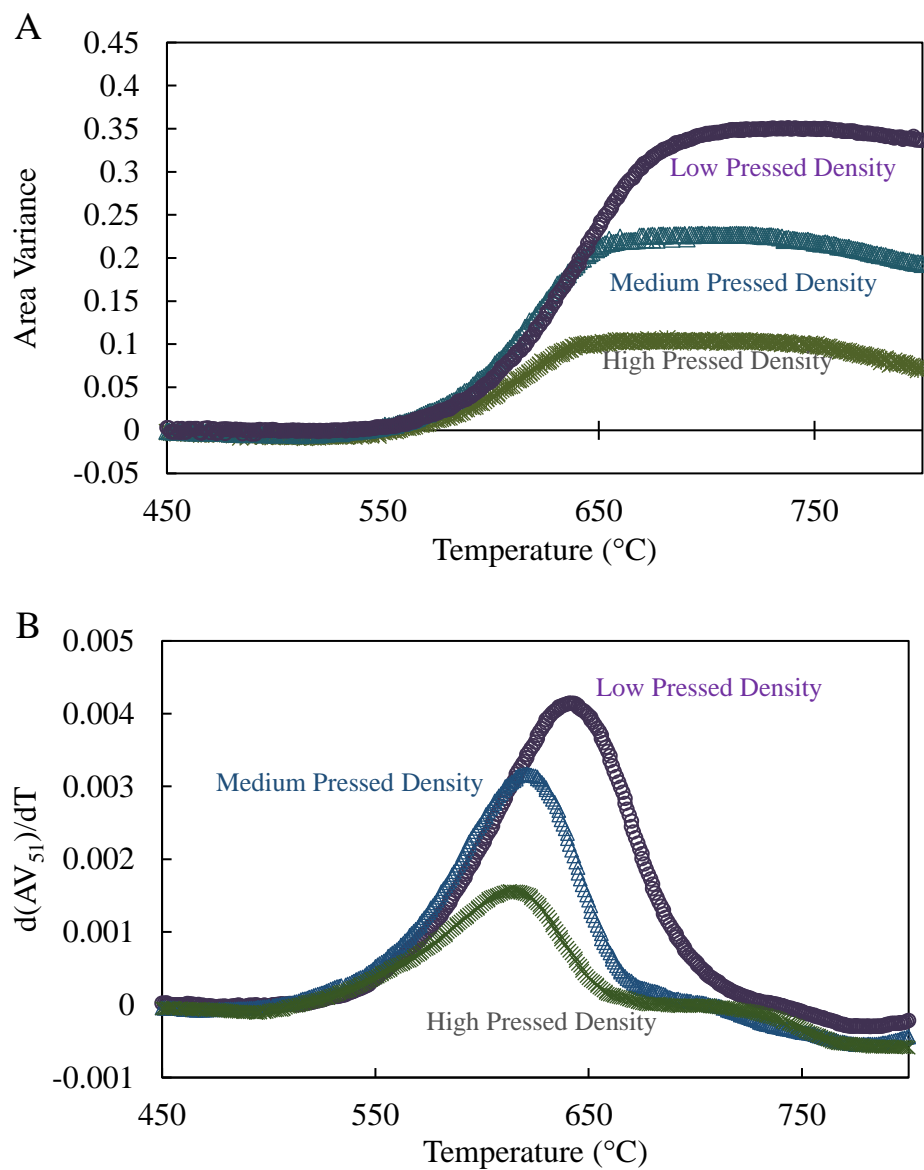
Figure 39. A) area variance as a function of temperature, B) $d(AV_{51})/dT$ as a function of temperature, for scalped powders of various pressed densities.
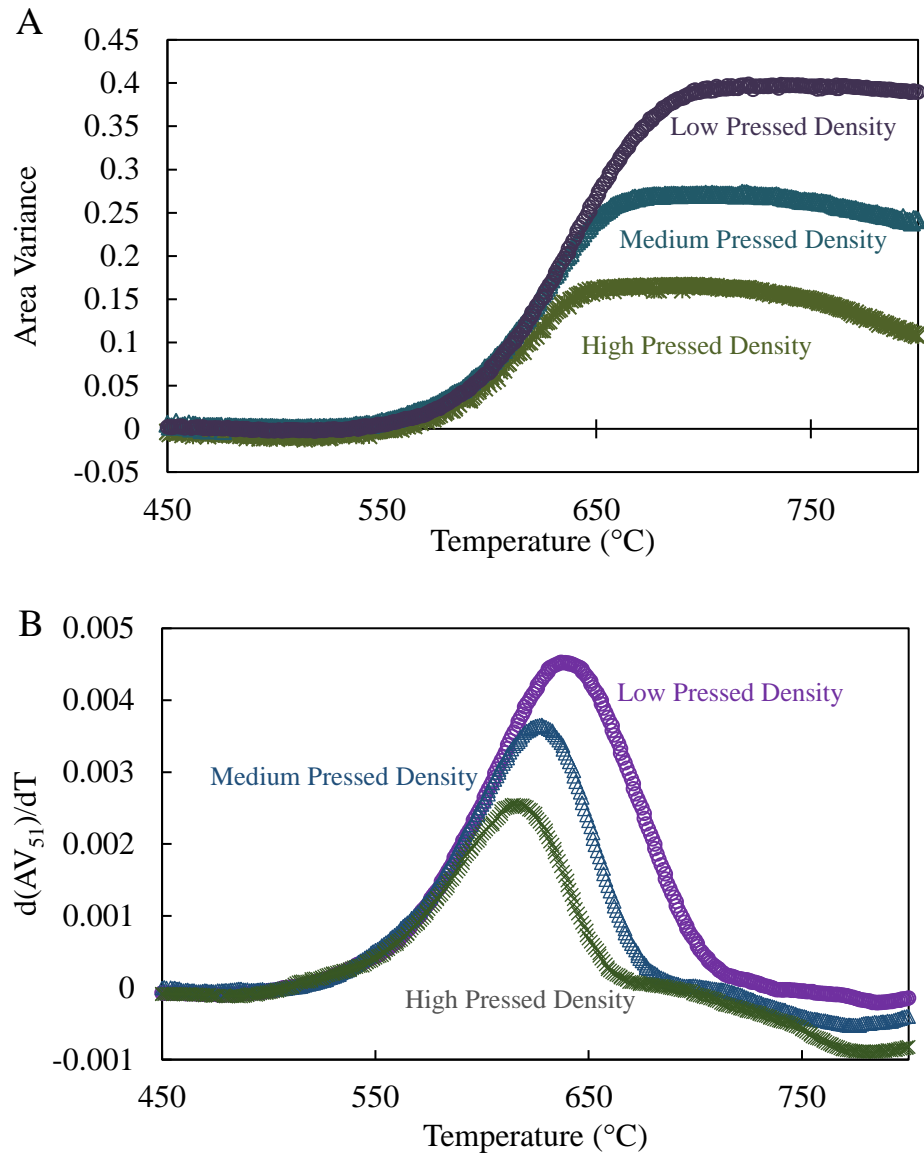
Figure 40. A) area variance and B) $d(AV_{51})/dT$ as a function of temperature for fine granules pressed to various relative densities.

Coarse granule compacts have greater area variances (shrinkages) for lower pressing densities (Figure 41A). However, the differences are much smaller than for scalped and fine granule compacts. The peak sintering temperature does not exhibit a shift of higher sintering temperatures for lower pressed densities (Figure 41B).
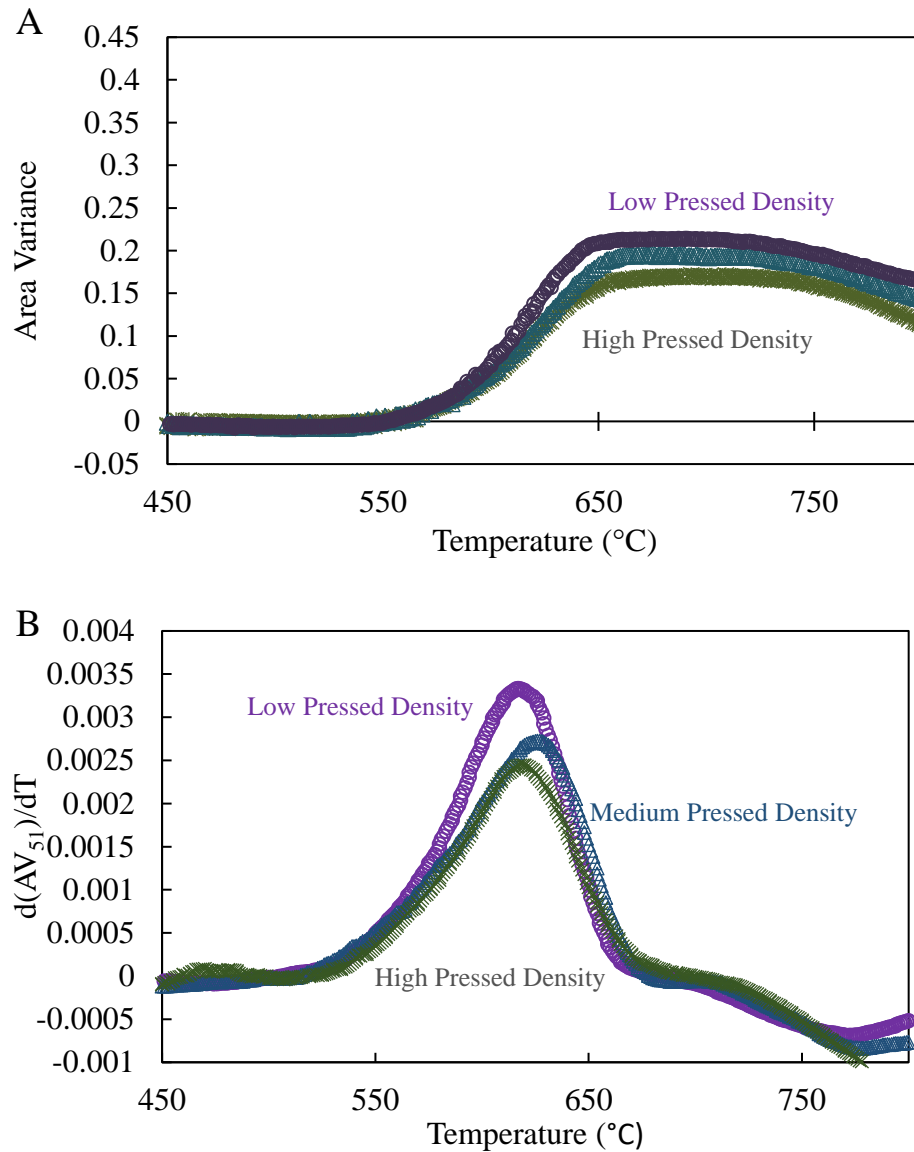
Figure 41. A) area variance and B) $d(AV_{51})/dT$ as a function of temperature for coarse powders pressed to various densities.

As relative density increases, peak sintering temperature decreases for fine and scalped powder compacts, as listed in Table IX and as seen in Figure 42. However, coarse granules behave differently. The peak sintering temperatures for coarse powders remain relatively constant with pressed density. It should be noted that the range of pressed heights, and therefore unsintered density, for coarse granules is smaller than that of scalped and fine granules. Concern for unsintered compact integrety of coarse granules resulted in greater stroke displacement (the strength of the pressed compacts is reduced for coarse powders).

Table IX. Peak sintering temperatures of blue glass compacts of various granule sizes ordered from low to high relative density.

Granule Distribution	Qualitative Pressed Density Relative to Granule Size	Relative Density %	Peak Sintering Temperature (°C)
fine	low	48.6 ± 0.21	641
scalped	low	52.2 ± 0.74	638
fine	medium	62.0 ± 0.79	628
scalped	medium	66.5 ± 0.79	626
coarse	low	67.3 ± 0.32	616
coarse	medium	70.8± 0.52	623
fine	high	74.2 ± 0.98	615
scalped	high	74.6 ± 1.3	616
coarse	high	74.8 ± 1.1	622
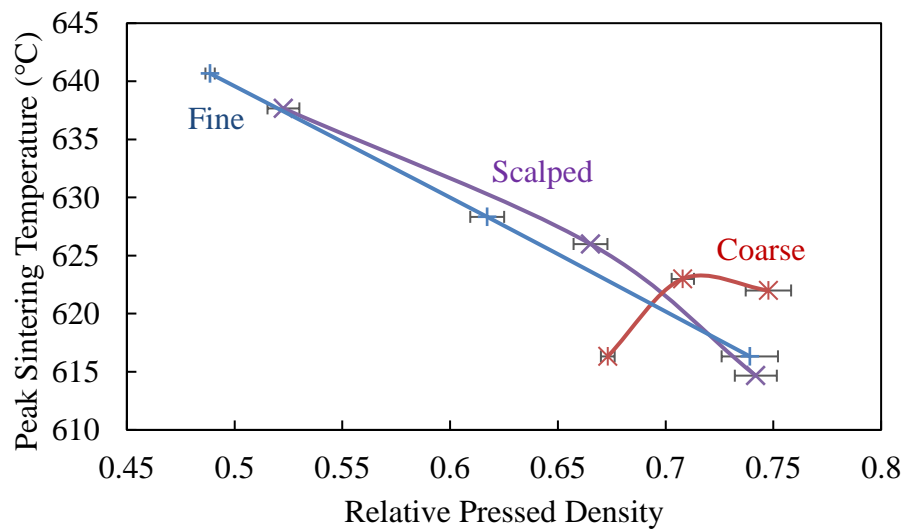
Figure 42. Blue glass peak sintering temperatures as a function of relative pressed density (% of theoretical). Samples, heated at 10 K/min, exhibited lower sintering temperatures for greater pressed densities, with the exception of coarse granules.

Coarse granules behave differently both during pressing and sintering. However, shrinkage is undoubtedly a function of pressed density for all granule size distributions.

CONCLUSIONS

Sintering occurs over a range of temperatures. Heating microscopy allows for the fast analysis of a cylindrical sample morphology as a function of temperature. The heating rates of non-isothermal sintering conditions are proven to alter the temperatures at which initial and final shrinkage occurs. These temperatures are also affected by pressed density and granule size. Lower pressed densities result in greater sintering temperatures for fine and scalped powders. Pressed density does not appear to have an effect on coarse granule sintering temperature.

HSM can provide information about the thermophysical behavior of materials. However, because of the limited resolution of the camera, certain conditions can lead to scattered data. Using pre-formed compacts pressed at a constant pressure improves the reliability and reproducibility of data between different samples. A data smoothing technique can also reduce the scatter when determining peak sintering temperature.

Various heating rates confirm that the thermal accumulation required for a powder compact to densify to a single monolithic form must be both temperature and time dependent. Sintering temperature appears to be a function of heating rate incorporating logarithmic time. Sintering temperatures of the observed glass samples, heated at constant heating rates with no dwell time, were observed to increase with increasing heating rates. The heat work required for a glass sample to sinter via viscous flow is approximately equivalent and constant for both blue and white glass, but decreases with increasing heating rate for borosilicate glass. Borosilicate glasses sinter at higher ratios of their glass transition temperatures that soda-lime silicates. Activation energy for the investigated borosilicate glass exceeds that of the silicate glasses. The comparisons of sintering behavior as a function of heating rate are only possible because of the similar initial densities within each dataset and composition. Therefore, revisions to the experimental procedures of the HSM manual are recommended.

SUGGESTIONS FOR FUTURE WORK

Though the samples used in this work have small volumes, a difference in heat work is demonstrated for borosilicate glass. It is proposed that because of a thermal gradient, which is feasible, less sintering (shrinkage) occurs for higher heating rates and therefore yielding differences in microstructure. To evaluate this effect, larger compacts, (1" diameter, 1" height) may be heated in a furnace with various heating rates and sectioned for microstructure analysis. Faster heating rates are proposed to have less shrinkage because the external surface will sinter faster, sealing the surface and trapping more porosity than slower heating rates. It is predicted that compacts experiencing faster heating rates yield lower densities (greater porosity) than slower heating rates.

Additionally, the final density of compacts is predicted depend on granule distribution and pressed density. Density measurements and microstructure analysis of porosity would determine the optimal granule size and pressing pressure for improved final densities.

REFERENCES

1.	Shelby, J. E., Glass Technology. In *Introduction to Glass Science and Technology*, 2 ed.; The Royal Society of Chemistry: Cambridge, UK, 2005; pp 249-261.

2.	Rabinovich, E., Preparation of glass by sintering. *Journal of Materials Science* **1985,** *20* (12), 4259-4297.

3.	Frenkel, J., Viscous flow of crystalline bodies under the action of surface tension. *Journal of Physics* **1945,** *9*, 385.

4.	Mackenzie, J.; Shuttleworth, R., A phenomenological theory of sintering. *Proceedings of the Physical Society. Section B* **1949,** *62* (12), 833.

5.	Kuczynski, G., Study of the sintering of glass. *Journal of Applied Physics* **1949,** *20* (12), 1160-1163.

6.	Kingery, W. D.; Berg, M., Study of the initial stages of sintering solids by viscous flow, evaporation-condensation, and self-diffusion. *Journal of Applied Physics* **1955,** *26* (10), 1205-1212.

7.	Panda, P. C.; Raj, R., Sintering and crystallization of glass at constant heating rates. *Journal of the American Ceramic Society* **1989,** *72* (8), 1564-1566.

8.	Pascual, M.; Pascual, L., Determination of the viscosity–temperature curve for glasses on the basis of fixed viscosity points determined by hot stage microscopy. *Physics and chemistry of Glasses* **2001,** *42* (1), 61-66.

9.	Fry, A. Sintering of Glass Frit. Master's Thesis, New York State College of Ceramics at Alfred University, Alfred, NY, 2017.

10.	Fluegel, A., Glass viscosity calculation based on a global statistical modelling approach. *Glass Technology-European Journal of Glass Science and Technology Part A* **2007,** *48* (1), 13-30.

11.	Scholze, H., Influence of viscosity and surface tension on hot-stage microscopy measurements on glasses. *Berichte der Deutschen Kermischen Gesellschaft* **1962,** *391*, 63-68.

12.	Pascual, M.; Durán, A.; Prado, M., A new method for determining fixed viscosity points of glasses. *Physics and Chemistry of Glasses* **2005,** *46* (5), 512-520.

13.	Schilm, J.; Rost, A.; Kusnezoff, M.; Megel, S.; Michaelis, A., Glass ceramics sealants for SOFC interconnects based on a high chromium sinter alloy. *International Journal of Applied Ceramic Technology* **2018,** *15* (2), 239-254.

14.	Fluegel, A. Statistical Calculation and Development of Glass Properties. glassproperties.com/viscosity/ (accessed August 28, 2021).

15.	Panna, W.; Wyszomirski, P.; Kohut, P., Application of hot-stage microscopy to evaluating sample morphology changes on heating. *Journal of Thermal Analysis and Calorimetry* **2016,** *125* (3), 1053-1059.

16.	Boccaccini, A. R.; Trusty, P. A., In situ characterization of the shrinkage behavior of ceramic powder compacts during sintering by using heating microscopy. *Materials Characterization* **1998,** *41* (4), 109-121.

17.	Venturelli, C., Heating Microscopy and its Applications. *Microscopy Today* **2011,** *19* (1), 20-25.

18.   Bordia, R. K.; Kang, S. J. L.; Olevsky, E. A., Current understanding and future research directions at the onset of the next century of sintering science and technology. *Journal of the American Ceramic Society* **2017,** *100* (6), 2314-2352.

19.   Rahaman, M., Theory of Solid-State and Viscous Sintering. In *Ceramic Processing and Sintering*, Marcel Dekker, Inc.: New York, NY, 1995; pp 374-444.

20.   Zagar, L. In *Theoretical aspects of sintering glass powders*, Sintering- New Developments, Dubrovnik, Yugoslavia, Sept. 5-10, 1977; Ristic, M. M., Ed. Elsevier Sci. Publishing Co.: Dubrovnik, Yugoslavia, 1977; p 57.

21.   Shimohira, T. M., K.; Kotani, K.; Wakakuwa, M. In *Sintering of monodispersed amorphous silica particles*, Factors in Densification and Sintering of Oxide and Non-Oxide Ceramic, Hakone, Japan, 1978-; Somiya, S. a. S., S., Ed. Gakujutusu Bunken Fukyu-Kai: Hakone, Japan, 1978; pp 119-127.

22.   Scherer, G. W.; Bachman, D. L., Sintering of low-density glasses: II, Experimental study. *Journal of the American Ceramic Society* **1977,** *60* (5-6), 239-243.

23.   Sacks, M. D.; Tseng, T. Y., Preparation of SiO2 glass from model powder compacts: II, sintering. *Journal of the American Ceramic Society* **1984,** *67* (8), 532-537.

24.   Kuczynski, G.; Zaplatynskyj, I., Sintering of glass. *Journal of the American Ceramic Society* **1956,** *39* (10), 349-350.

25.   Scherer, G. W., Sintering of low-density glasses: I, theory. *Journal of the American Ceramic Society* **1977,** *60* (5-6), 236-239.

26.   German, R. M., Solid State Sintering Fundamentals. In *Sintering Theory and Practice*, John Wiley & Sons, Inc.: New York, NY, 1996; pp 68-72.

27.   Kingery, W., Regelation, surface diffusion, and ice sintering. *Journal of Applied Physics* **1960,** *31* (5), 833-838.

28.   Exner, H. E.; Arzt, E., Sintering processes. *Sintering Key Papers* **1990**, 157-184.

29.   Exner, H.; Petzow, G., Shrinkage and rearrangement during sintering of glass spheres. In *Sintering and Catalysis*, Springer: 1975; pp 279-293.

30.   Scherer, G. W., Sintering of low-density glasses: III, Effect of a distribution of pore sizes. *Journal of the American Ceramic Society* **1977,** *60* (5-6), 243-246.

31.   Geguzin, Y. E.; Kruzhanov, V., Sintering of amorphous spheres. *Soviet Powder Metallurgy and Metal Ceramics* **1972,** *11* (5), 367-371.

32.   Cutler, I. B., Sintering of glass powders during constant rates of heating. *Journal of the American Ceramic Society* **1969,** *52* (1), 14-17.

33.   Karamanov, A.; Aloisi, M.; Pelino, M., Sintering behaviour of a glass obtained from MSWI ash. *Journal of the European Ceramic Society* **2005,** *25* (9), 1531-1540.

34.   Starink, M., The determination of activation energy from linear heating rate experiments: a comparison of the accuracy of isoconversion methods. *Thermochimica Acta* **2003,** *404* (1-2), 163-176.

35.   Karamanov, A.; Dzhantov, B.; Paganelli, M.; Sighinolfi, D., Glass transition temperature and activation energy of sintering by optical dilatometry. *Thermochimica Acta* **2013,** *553*, 1-7.

36.   Chen, H. S., A method for evaluating viscosities of metallic glasses from the rates of thermal transformations. *Journal of Non-Crystalline Solids* **1978,** *27* (2), 257-263.

37.   Scherer, G. W., Viscous Sintering with a Pore-Size Distribution and Rigid Inclusions. *Journal of the American Ceramic Society* **1988,** *71* (10), C447-C448.
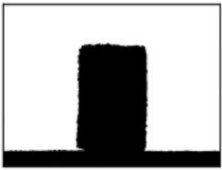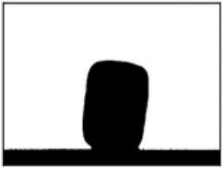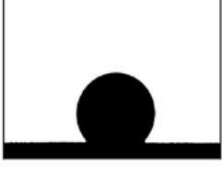
38.   Scherer, G. W., Viscous sintering of a bimodal pore-size distribution. *Journal of the American Ceramic Society* **1984,** *67* (11), 709-715.

39.   Cutler, I. B., Effect of water vapor on the sintering of glass powder compacts. *Journal of the American Ceramic Society* **1969,** *52* (1), 11-13.

40.   Geguzin, Y. E., Sintering of particles of nonspherical shape. *Soviet Powder Metallurgy and Metal Ceramics* **1967,** *6* (5), 364-367.

41.   Prado, M.; Fredericci, C.; Zanotto, E. D., Glass sintering with concurrent crystallisation. Part 2. Nonisothermal sintering of jagged polydispersed particles. *Physics and Chemistry of Glasses* **2002,** *43* (5), 215-223.

42.   Prado, M. O.; Fredericci, C.; Zanotto, E. D., Isothermal sintering with concurrent crystallization of polydispersed soda–lime–silica glass beads. *Journal of Non-Crystalline Solids* **2003,** *331* (1-3), 145-156.

43.   Prado, M. O.; Fredericci, C.; Zanotto, E. D., Non-isothermal sintering with concurrent crystallization of polydispersed soda–lime–silica glass beads. *Journal of Non-Crystalline Solids* **2003,** *331* (1-3), 157-167.

44.   Prado, M. O.; Zanotto, E. D.; Müller, R., Model for sintering polydispersed glass particles. *Journal of Non-Crystalline Solids* **2001,** *279* (2-3), 169-178.

45.   Reis, R. M.; Barbosa, A. J.; Ghussn, L.; Ferreira, E. B.; Prado, M. O.; Zanotto, E. D., Sintering and rounding kinetics of irregular glass particles. *Journal of the American Ceramic Society* **2019,** *102* (2), 845-854.

46.   Prado, M. O.; Zanotto, E. D.; Fredericci, C., Sintering polydispersed spherical glass particles. *Journal of Materials Research* **2003,** *18* (6), 1347-1354.

47.   Soares, V. O.; Reis, R. C.; Zanotto, E. D.; Pascual, M. J.; Durán, A., Non-isothermal sinter-crystallization of jagged Li2O–Al2O3–SiO2 glass and simulation using a modified form of the Clusters model. *Journal of Non-Crystalline Solids* **2012,** *358* (23), 3234-3242.

48.   Giess, E. A.; Fletcher, J. P.; Herron, L. W., Isothermal sintering of cordierite-type glass powders. *Journal of the American Ceramic Society* **1984,** *67* (8), 549-552.

49.   Cutler, I. B.; HenrichSen, R. E., Effect of particle shape on the kinetics of sintering of glass. *Journal of the American Ceramic Society* **1968,** *51* (10), 604-604.

50.   Prado, M. O.; Nascimento, M. L. F.; Zanotto, E. D., On the sinterability of crystallizing glass powders. *Journal of Non-Crystalline Solids* **2008,** *354*, 9.

51.   Prado, M. O.; Ferreira, E. B.; Zanotto, E. D., Sintering kinetics of crystallizing glass particles. A review. *Melt Chemistry, Relaxation, and Solidification Kinetics of Glasses* **2006,** *170*, 163-179.

52.   Prado, M. O.; Zanotto, E. D., Glass sintering with concurrent crystallization. *Comptes Rendus Chimie* **2002,** *5* (11), 773-786.

53.   Zanotto, E. D., Surface crystallization kinetics in soda-lime-silica glasses. *Journal of Non-Crystalline Solids* **1991,** *129* (1-3), 183-190.

54.   Zanotto, E. D., Glass Crystallization Research—A 36-Year Retrospective. Part I, Fundamental Studies. *International Journal of Applied Glass Science* **2013,** *4* (2), 105-116.

55.   Petzow, G.; Exner, H. E., Particle rearrangement in solid state sintering. In *Sintering Key Papers*, Springer: 1990; pp 639-655.

56.   Shelby, J. E., Viscosity of Glass Forming Melts. In *Introduction to Glass Science*, 2 ed.; The Royal Society of Chemistry: Cambridge, UK, 2005; pp 111-137.

57.	Zheng, Q.; Mauro, J. C., Viscosity of glass-forming systems. *Journal of the American Ceramic Society* **2017,** *100* (1), 6-25.

58.	Varshneya, A. K., The Viscosity and Surface Tension of Glass. In *Fundamentals of Inorganic Glasses*, 2 ed.; Society of Glass Technology: Sheffield, 2013; pp 213-247.

59.	Doremus, R. H., Viscosity. In *Glass Science*, John Wiley & Sons, Inc.: New York, NY, 1973; pp 101-114.

60.	Fluegel, A., Thermal expansion calculation for silicate glasses at 210 C based on a systematic analysis of global databases. *Glass Technology-European Journal of Glass Science and Technology Part A* **2010,** *51* (5), 191-201.

61.	Moynihan, C. T.; Easteal, A. J.; Wilder, J.; Tucker, J., Dependence of the glass transition temperature on heating and cooling rate. *The Journal of Physical Chemistry* **1974,** *78* (26), 2673-2677.

62.	Kuppinger, C. M.; Shelby, J. E., Viscosity and thermal expansion of mixed-alkali sodium-potassium borate glasses. *Journal of the American Ceramic Society* **1985,** *68* (9), 463-467.

63.	Boccaccini, A.; Hamann, B., Review in situ high-temperature optical microscopy. *Journal of Materials Science* **1999,** *34* (22), 5419-5436.

64.	Zanotto, E. D.; Mauro, J. C., The glassy state of matter: Its definition and ultimate fate. *Journal of Non-Crystalline Solids* **2017,** *471*, 490-495.

65.	Mazurin, O., Problems of compatibility of the values of glass transition temperatures published in the world literature. *Glass Physics and Chemistry* **2007,** *33* (1), 22-36.

66.	Fulcher, G. S., Analysis of recent measurements of the viscosity of glasses. *Journal of the American Ceramic Society* **1925,** *8* (6), 339-355.

67.	Kamseu, E.; Rizzuti, A.; Miselli, P.; Veronesi, P.; Leonelli, C., Use of noncontact dilatometry for the assessment of the sintering kinetics during mullitization of three kaolinitic clays from Cameroon. *Journal of Thermal Analysis and Calorimetry* **2009,** *98* (3), 757-763.

68.	Lara, C.; Pascual, M. J.; Prado, M.; Durán, A., Sintering of glasses in the system RO–Al2O3–BaO–SiO2 (R= Ca, Mg, Zn) studied by hot-stage microscopy. *Solid State Ionics* **2004,** *170* (3-4), 201-208.

69.	Yang, G.; Migone, A.; Johnson, K., Heat capacity and thermal diffusivity of a glass sample. *Physical Review B* **1992,** *45* (1), 157.

70.	Laubitz, M., Thermal conductivity of powders. *Canadian Journal of Physics* **1959,** *37* (7), 798-808.

71.	Kanjanapant, A., Private Communication ed.; Elan Technologies: Midway, GA, 2021.

72.	Dolson, J. Precision Glass GTMS Sealing Component Specialists. https://www.richlandglass.com/wp-content/uploads/2019/04/GTMS-Lit_042519.pdf (accessed July 1, 2021).

73.	Hsieh, P. Y., Viscous deformation as a measure of heat work during coal ash fusibility testing. *Fuel* **2020,** *281*, 118723.

74.	Hsieh, P. Y., Effects of temperature non-uniformity and effective viscosity on pyrometric cone deformation. *International Journal of Ceramic Engineering & Science* **2019,** *1* (4), 216-226.

75.   Lerdprom, W. Firing of porcelain. Masters Thesis, New York State College of Ceramics at Alfred University, Alfred, NY, 2014.

76.   Reed, J. S., Pressing. In *Principles of Ceramic Processing*, 2nd ed.; John Wiley & Sons, Inc.: New York, NY, 1995; pp 418-449.

APPENDIX

Onset of data acquisition:
The image analyzer automatically takes as 100% the height of the sample, measured considering the sample holder (alumina support) as a base reference.

Sintering:
As the temperature increases, the viscous flow activation threshold is overcome and the material undergoes the sintering phase: the sample decreases in size, but its shape does not substantially change. In the case of glasses, glazes, and frits, the driving force of the sintering process is the surface tension of the vitreous phases. The sintering phase ends when the sample reaches its maximum density. The sintering temperature identified by the instrument is the temperature at which the sample has reached a dimensional variation corresponding to the 5% with respect to the first image acquired, which is taken to be 100%.

Softening:
The softening point is reached when liquid phases appear on the surface of the sample. From this point on, the shape of the sample undergoes substantial changes caused by the surface tension of the liquid phases. To find this point, the rounding of the corners of the sample and the smoothing of the upper part of the walls of the sample are taken into consideration.

Sphere:
At the sphere temperature the sample is formed almost entirely of liquid phases, and the shape of the sample is controlled by the surface tension. While the surface tension tends to reduce the surface to a minimum forming a sphere, the hydrostatic pressure related to the density of the liquid phase tends to flatten the shape. Some glasses do not reach the sphere point: for example, glasses with a high density and a low surface tension (lead silicates).
In detecting the sphere temperature, every image analyzed is compared with a theoretical sphere.

Half Sphere:
The half sphere temperature is reached when the height of the sample is half the width of the base. If the glass behaves normally, at the half sphere temperature the contact angle is approximately 90°. However, at this temperature the contact angle is often much higher, and in some cases the shape of the sample can resemble a bell. These anomalies can be attributed to the formation of non-homogenous phases inside the sample, such as crystallization or glass-glass separations.

Melting:
When the height of the sample shrinks to under a third of the base, it is assumed that the sample has completely liquified and has reached the melting point.

Appendix Figure 1. Misura ® HSM definition of characteristic points.[17]